# Synthesis of ZIF-67 based ternary NiMnCo/NPC as an electro-catalyst for methanol oxidation reaction



By

**Aqsa Saqib Lodhi**

**Reg. No. 00000318950**

**Session 2019-21**

**Supervised by**

**Dr. Naseem Iqbal**

**A Thesis Submitted to the US-Pakistan Center for Advanced Studies in Energy in partial fulfillment of the requirements for the degree of**

**MASTER of SCIENCE in**

**Energy Systems Engineering**

**US-Pakistan Center for Advanced Studies in Energy (USPCAS-E)**

**National University of Sciences and Technology (NUST)**

**H-12, Islamabad 44000, Pakistan**

**June 2022**

# THESIS ACCEPTANCE CERTIFICATE

Certified that final copy of MS/MPhil thesis written by **Ms. Aqsa Saqib Lodhi** (Registration No. <u>00000318850</u>), of US-Pakistan Center for Advanced Studies in Energy (USPCAS-E) has been vetted by undersigned, found complete in all respects as per NUST Statues/Regulations, is within the similarity indices limit and is accepted as partial fulfillment for the award of MS degree. It is further certified that necessary amendments as pointed out by GEC members of the scholar have also been incorporated in the said thesis.

Signature: _____

Name of Supervisor: _____

Date: _____


Signature (HOD): _____

Date: _____


Signature (Dean/Principal): _____

Date: _____

# Certificate

This is to certify that work in this thesis has been carried out by **Ms. Aqsa Saqib Lodhi** and completed under my supervision in Synthesis and Energy Storage laboratory, US-Pakistan Center for Advanced Studies in Energy (USPCAS-E), National University of Sciences and Technology, H-12, Islamabad, Pakistan.

Supervisor: _____

Prof. Dr. Naseem Iqbal

USPCAS-E

NUST, Islamabad

GEC member 1: _____

Dr. Ghulam Ali

USPCAS-E

NUST, Islamabad

GEC member 2: _____

Dr. Mustafa Anwar

USPCAS-E

NUST, Islamabad

GEC member 3: _____

Dr. Nadia Shahzad

USPCAS-E

NUST, Islamabad

HOD-ESE: _____

Dr. Rabia Liaquat

USPCAS-E

NUST, Islamabad

Dean/Principal:

Prof. Dr. Adeel Waqas

USPCAS-E

NUST, Islamabad

# Dedication

*To my parents, who supported me in every aspect of life and my siblings.*

# Acknowledgments

First and foremost, I am thankful to Almighty ALLAH who is the creator and author of knowledge. Indeed, without YOUR blessings, this mammoth task would not have been possible. And I acknowledge that without YOUR willingness and guidance, I would not have done a single task.

I am grateful to my parents for their unconditional love and sacrifices. I am forever in your debt for your encouragement, financial and moral support. Thank you for keeping confidence in me.

**Dr. Naseem Iqbal**, I express my sincerest gratitude to you for this opportunity, for your teaching, mentorship, and patience throughout the research. It has been truly a privilege to work with you. I would like to thank my GEC members **Dr. Ghulam Ali, Dr. Mustafa Anwar,** and **Dr. Nadia Shahzad** for their guidance and help throughout my research.

I am also thankful to the staff of Synthesis and Energy Storage Lab specially **Engineer Naveed,** who helped in my research and gave valuable advice during my experimentation. I am also grateful to the other lab staff, faculty members, and administration who were a part of this journey. I profusely thank my mother **Nadia Hamid Lodhi** for her immense support, always being there for me whenever I needed help. Also, all my seniors and my friends Neelam Zaman, Midhat Naveed, Hira Anwar for their support both academically and in general. And to life, an extraordinary experience with so many things to enjoy within a short span. Thank you for giving me so much in the years past, and for more to discover in the years to come.

# Abstract

The extreme energy depletion has negative effects for the global ecosystem. Environmental pollution has become a serious concern throughout the world as a result of the fast depletion and usage of fossil fuels. Fuel cells are being considered as a viable alternative to fossil fuels as a source of energy. Among all fuel cell, direct methanol fuel cells (DMFCs) have aroused a lot of attention due to their low operating temperature and excellent energy conversion efficiency. The effectiveness of the methanol oxidation process (MOR) utilized in DMFCs have significant effect on their performance. Catalytic activity of catalysts is heavily reliant on their surface structure; hence, improving the efficiency of the methanol oxidation reaction (MOR) necessitates surface structure modification.

In this study, the electrocatalytic activity of mono-metallic Co/NPC, bi-metallic MnCo/NPC, and ternary NiMnCo/NPC in alkaline media for the methanol oxidation reaction (MOR) was examined. These materials were produced using a simple solution mixing method and characterized using FTIR, EDX, SEM, XPS, TGA and XRD. The SEM and TEM results showed the presence of Nanoporous carbon. Als o the XRD results showed the formation of graphitic carbon. In a three-electrode arrangement, on glassy carbon electrodes, the investigation of methanol oxidation for electrochemical activity of catalysts was carried in 1 M NaOH and 3 M $CH_3OH$. Electrochemical studies included cyclic voltammetry (CV), chronoamperometry (CA), and electron impedance spectroscopy (EIS). The ternary NiMnCo/NPC composite, which has a peak current density of 147.85 mA/cm$^2$ at 0.8 potential and a scan rate of 50 mV/s among all the composites developed, also chronoamperometry results showed that the stability is 55.83%, proving it is a promising catalyst for methanol electrocatalysis.

**Keywords:** Methanol oxidation reaction (MOR), Bi-metallic ZIF, Ternary ZIF, Nano porous carbon (NPC)

# Table of Contents

# List of Figures

# List of Tables

# List of Publications

1. Aqsa Saqib Lodhi, Naseem Iqbal, Tayyaba Noor, Neelam Zaman, Junko Gao, "ZIF-67 derived Ternary NiMnCo based Nanoporous Carbon Material for Methanol Oxidation Reaction**." International Journal of Energy Research, 2022**

# List of Abbreviations

| | |
|---|---|
| MOR | Methanol Oxidation reaction |
| FC | Fuel cell |
| SOFC | Solid oxide fuel cell |
| AFC | Alkaline fuel cell |
| PEMFC | Polymer electrolyte membrane fuel cell |
| MCFC | Molten carbonate fuel cell |
| DMFC | Direct methanol fuel cell |
| MOF | Metal organic framework |
| ZIF | Zeolite imidazole framework |
| CA | Chronoamperometry |
| CV | Cyclic Voltammetry |
| XRD | X ray Diffraction |
| XPS | X ray photoelectron spectroscopy |
| SEM | Scanning Electron Microscopy |
| EIS | Electrochemical impedance spectroscopy |
| TEM | Transmission electron microscope |
| FTIR | Fourier transform infrared spectroscopy |
| EDS | Energy dispersive X-ray spectroscopy |
| V | Voltage |
| PAFC | Phosphoric Acid Fuel Cell |
| Km | Kilometers |
| HER | Hydrogen Evolution Reaction |
| ORR | Oxygen Reduction Reaction |

# Chapter 1:

# Introduction

Energy spending is a representation of a country's industrial growth and success since energy is a crucial part of almost all development and activities. Due to rising populations and higher living standards, traditional energy supplies such as fossil fuels have been increasingly depleted in recent decades[1, 2]. Furthermore, this extreme energy depletion has negative effects for the global ecosystem. Environmental pollution has become a serious concern throughout the world as a result of the fast depletion and usage of fossil fuels[3].

## 1.1 Energy Crisis

When looking at current global energy utilization from the perspective of long-term recorded patterns, the last 150 years appear to have been a remarkable but impractical period: remarkable in terms of improved comfort and ways of life, but unreasonable in terms of the environmental change that has occurred[4]. The current commercial speed is 1,000 kilometers per hour, yet moving electronic data to any location on the earth takes only a few seconds. We are currently experiencing, albeit slowly, a pause in late progress: all types of pollution are wreaking havoc on the planet, and the current situation is most likely unjustifiable, especially when asset shortages and segment development are taken into account[5]. Indeed, only a small number of people are directly and seriously harmed by environmental change. Whatever the case may be, the year 2006 appeared to be a watershed point in the public's awareness of the situation. A few components of the combined energy-climate dilemma have crystallized in some way. The world has truly become a global village[6]. The challenges of achieving global financial stability and an acceptable standard of living in a society with an ever-growing population and varying degrees of wealth and social imbalance are mind-boggling and enormous. The link between man and machine, efficiency, and the current course of events continues. Whether in the purportedly formed countries' urban centers or in the rapidly expanding metropolitan populated communities of the emerging scene, concern

for the air that sustains Earth's biological system is becoming increasingly important. Air quality has an impact on the environment's overall balance and extreme well-being. It is instructive to take a minute to consider the composition and organization of Earth's air, as well as the tremendous pretended via carbonaceous forces throughout mankind's history. The use of the renewable energy has gained great importance during the last 10 years due to environmental hazards caused by the conventional sources and the depletion of fossil fuels[7, 8].
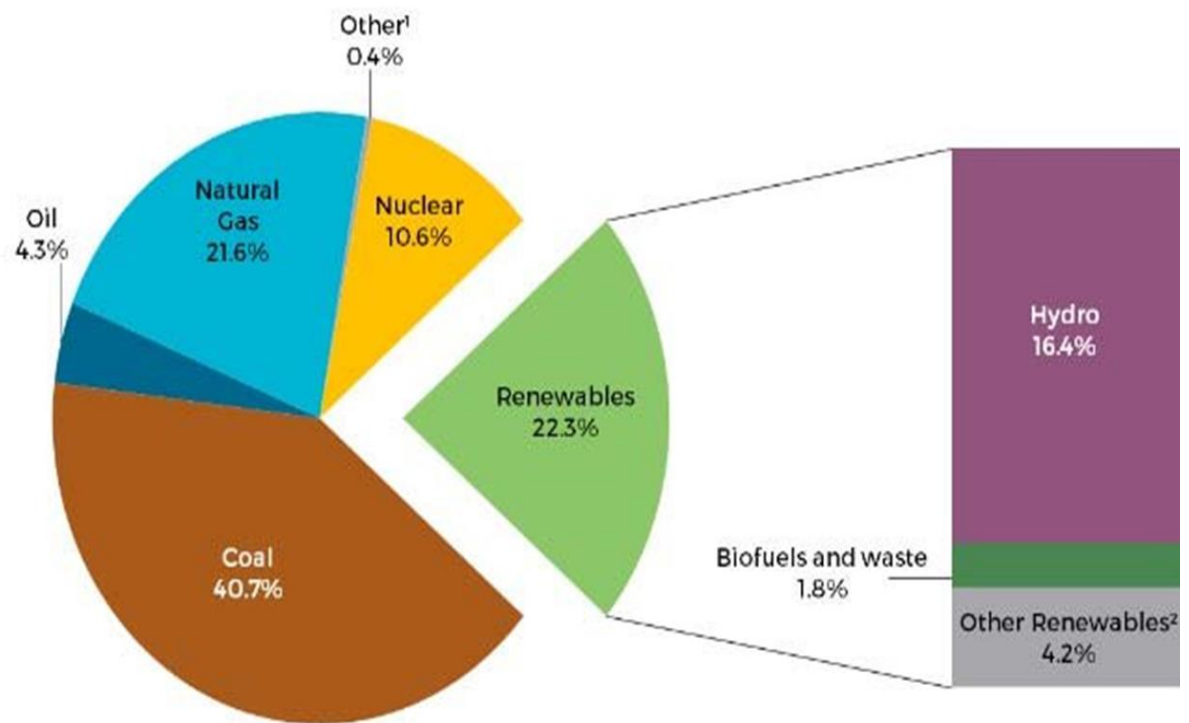


Figure 0.1  Illustrative diagram of various renewable energy resources

## 1.2 Fuel Cell

Fuel cells are being considered as a viable alternative to fossil fuels as a source of energy. Fuel cells are interesting candidates for supplying energy to modern portable electric cars and electronic gadgets in a sustainable and efficient manner[9]. Fuel (MeOH, Ethanol, and molecular $H_2$) at the anode and molecular $O_2$ at the cathode undergo a catalytic reaction, which turns chemical energy into electrical energy via electrochemical processes[10]. These cells have shown to be excellent energy

conversion devices, ensuring adequate electrical energy for power system. Despite the early focus of fuel cell development was on massive production, with the eventual goal of developing 200–300 kW energy cells, there is currently a lot of focus on smaller fuel cells[11].

## 1.2.1 Types of Fuel Cells

There are six major types of energy components at varying stages of company accessibility or examination/improvement at this time. Even while different energy units function on similar substance reactions, they are nonetheless vastly varied in terms of operating characteristics, materials used in construction, and applicability.

They include[11];

> ➢ Alkaline fuel cells (AFC)
> ➢ Proton exchange membrane fuel cells (PEMFC)
> ➢ Phosphoric acid fuel cells (PAFC)
> ➢ Solid oxide fuel cells (SOFCs)
> ➢ Molten carbonate fuel cells (MCFC)
> ➢ Direct methanol fuel cells (DMFC)

## 1.2.1.1 DMFC

Methanol is used as a source of energy in this technique. A DMFC has an anode where methanol is electro-oxidized to $CO_2$ and a cathode where oxygen (typically in the form of air) is reduced to water or steam. Methanol is used as fuel which converts stored chemical form of energy in methanol into electrical energy via oxidation. Due to the usage of methanol as fuel it is different from all available fuel cells[20].

**At Anode**

$$CH_3OH + H_2O \rightarrow CO_2 + 6H^+ + 6\bar{e} \tag{1}$$

**At Cathode**

$$3/2O_2 + 6H^+ + 6\bar{e} \rightarrow 3H_2O \tag{2}$$
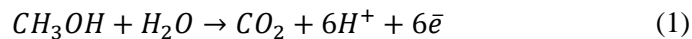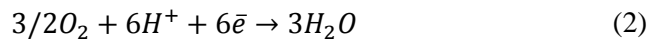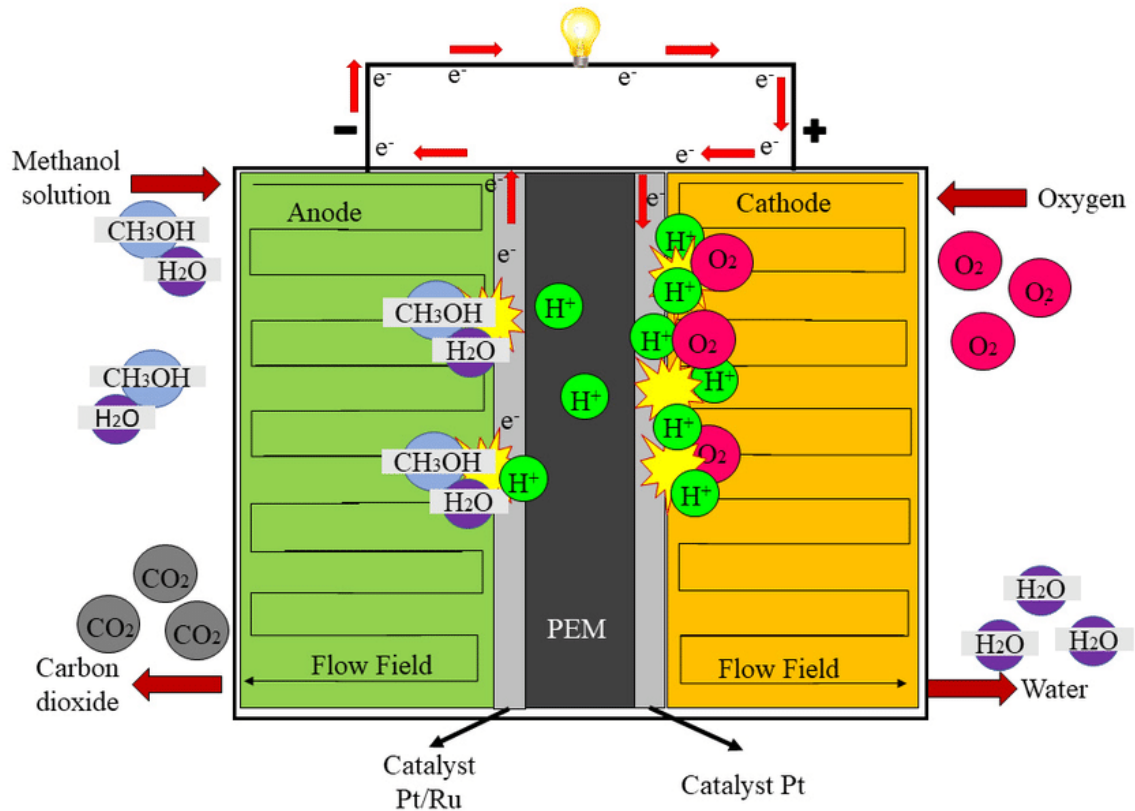
Figure 0.2 Illustrative diagram of DMFC

Because methanol has a higher specific energy density than lithium-polymer, li-ion polymer systems, and other best rechargeable batteries. The DMFC has the power to substitute the battery. In contrast to rechargeable batteries, that might take hours to restore a depleted power pack, the fuel in a DMFC can be changed in less time [21].

**1.2.1.1.1 Challenges in DMFC**

The greatest theoretical voltage a fuel cell can function depends on its operating temperature. Lower theoretical maximum voltages and efficiency are associated with higher temperatures. Higher temperatures at the electrodes, on the other hand, boost electrochemical activity, increasing efficiency. The quality of waste heat is improved by operating at a greater temperature. It's worth noting that a given type of fuel cell can only work well and dependably within a certain temperature range. A fuel cell that uses methanol as a fuel[22].

An overview of various fuel cell technology types illustrating reaction conditions such as fuel, temperature and reaction mechanism is shown in Figure 1.3.
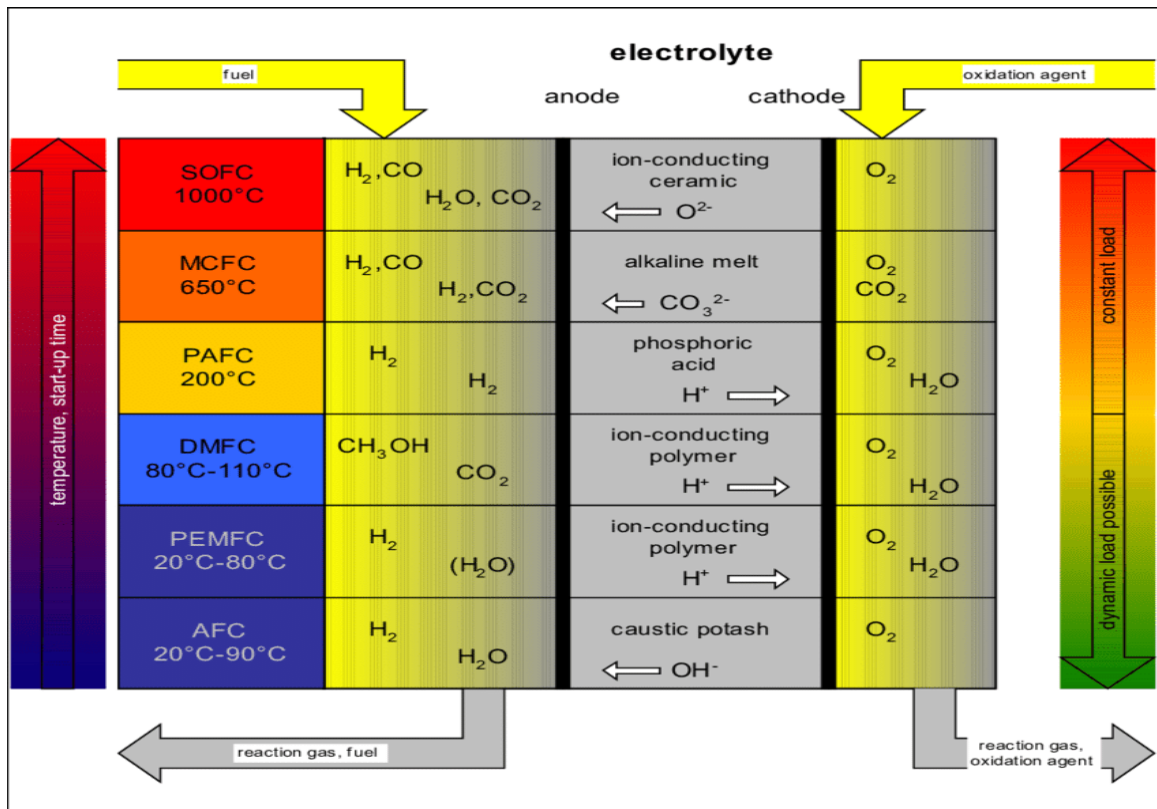
Figure 0.3  Illustrative diagram of comparison of various fuel cell

## 1.3 MOFs

Metal organic frameworks (MOF) are the hybrid crystalline Inorganic-Organic materials that are made up of positively charged metal that is surrounded by the linkers. Metal ions produce nodes, which connect the linkers to form a cage-like structure[23]. However, the majority of MOFs can't be used as electrocatalysts straight away, due to their weak chemical resistance and low electrical conductivity stability. As a result, pyrolysis was used to transform MOFs into a variety of conductive carbon-based compounds[25]. Some of the structural advantages of MOFs, including as large surface area, can be passed down to the resultant materials[26, 27].
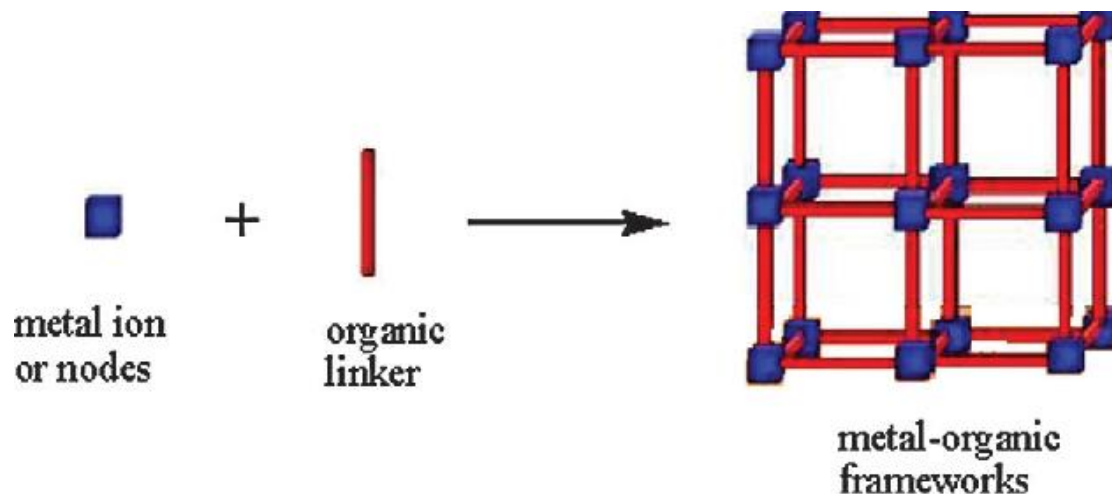
Figure 0.4   Illustrative diagram of metal organic framework

Many Scientists shows that characteristics of MOFs can be controllable by varying linker and metal [28]. The structure of MOFs depend on the choice of ligands and metal so the architecture can be controlled accordingly. Due to numerous possible combinations, a number of metal organic frameworks has been reported which can be customized according to the applications for which they are used. So, the metals and organic linkers present in metal organic framework should in accordance with the applications that need to be performed. By keeping in mind this point we can even get good efficiency and performance by these MOFs[29].
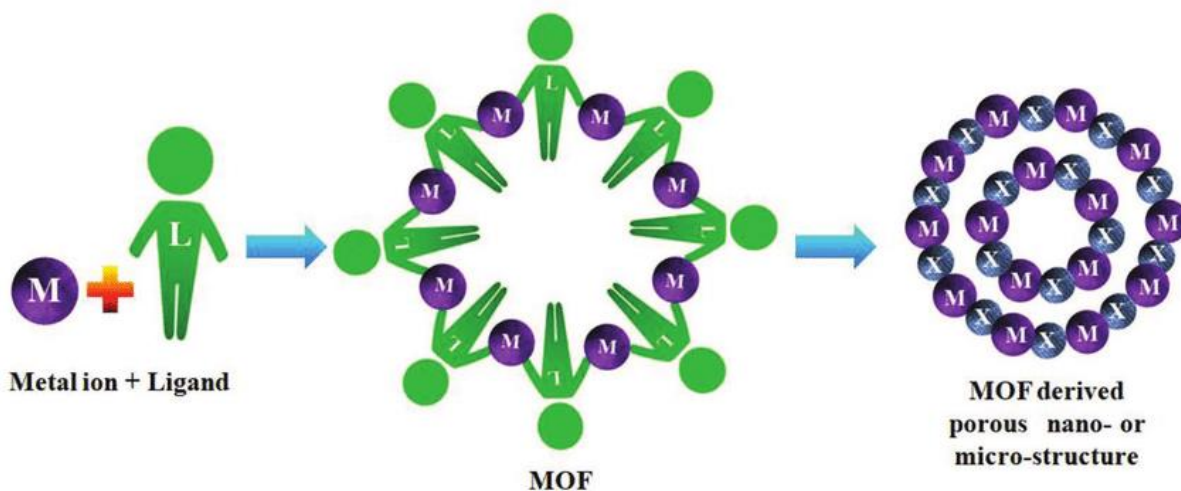


Figure 0.5   Illustrative diagram of MOF derived nano porous structure

## 1.4 Zeolite Imidazole Framework (ZIF)

ZIFs are made up of 4-, 6-, 8-, or 12-membered-ring tetrahedral clusters formed by transition metal (e.g., Zn, Co) bridged N atoms via imidazolate (MIM) units or functionalized MIM, resulting in an extended framework with tunable nanopores[20,21]. ZIFs exhibit exceptional zeolitic and metal-organic framework (MOF) characteristics, garnering the interest of many researchers. In comparison to other MOFs, ZIFs exhibit superior mechanical and chemical stability thanks to their stable metal-nitrogen connections[31].

### 1.4.1 Strategies for synthesis of ZIF

There have been several strategies for the production of ZIFs documented thus far. The most often described methods of manufacture are liquid-phase, in which either an imidazole or a metal solution is combined separately, or the addition of a suitable solvent to a metal and ligand combination. Solvent selection for liquid-phase processes is influenced by a number of characteristics, including redox potential, stability constant, solubility, and reactivity. Solvent has an important influence in determining activation energy and thermodynamics[32].

Many researchers have indicated formation of ZIF in solid matrix since it is easier and faster, although solid phase synthesis is challenging to get single crystals, which is very straightforward in liquid phase.

Synthesis of ZIFs involves the following widely used methods[33]:

> ➢ Simple Solution Mixing
> ➢ Solvothermal
> ➢ Microwave-assisted
> ➢ Electrochemical
> ➢ Mechanochemical
> ➢ Sono-chemical

### 1.4.1.1  Simple Solution Mixing

The reaction may be completed without using any external heat in this approach. In most cases, a magnetic stirrer is used to combine the imidazole and metal solutions. If a product is produced, it will precipitate if it is washed with alcohols and then dried in the oven[34].

### 1.4.1.2. Solvothermal

Reactions are carried out in a closed vessel with an internal pressure greater than the boiling point of the solvent. Under such circumstances, a variety of unexpected changes in precursors occur that can never be produced using traditional approaches, resulting in nanoscale morphologies. The choice of solvent is determined by the solubility of the starting components; however, if required, a combination of solvents can be utilized. DMF, acetonitrile, diethyl formamide, methanol, ethanol, acetone, and other organic solvents are often utilized. Depending on the demands of the reactions, these reactions are conducted at various temperatures. Glass-lined autoclaves are often used for low-temperature process reactions, whereas Teflon-lined autoclaves are required for higher-temperature reactions. This hydrothermal method has been utilized to create a wide variety of hybrid materials[35].

### 1.4.2 Applications of ZIFs

When it comes to energy generation, gases are a highly helpful source, thus having some decent storage tanks is a must. Many choices exist for this purpose, but some of them need multi-stage compressors, high-pressure tanks, or are too expensive to be practical, necessitating the development of a more dependable, less expensive storage mechanism. ZIF is the most commonly studied and utilized material, since it not only acts as a gas storage and separation option, but also as a source of clean transportable energy. ZIFs have a number of advantages over other porous materials, including simple synthetic methods, changeable functionalization, adjustable pore size, and a large surface area. As a result, several ZIF traits emerge[44].

The different applications of ZIFs are given below:

- ➢ ZIFs for Catalysis
- ➢ ZIFs for Sensors
- ➢ ZIFs for Microwave Absorption
- ➢ ZIFs for Electro-chemistry

### 1.4.2.1 ZIFs for Catalysis

Catalysts capable of great performance while staying ecologically safe are crucial for the expansion of any sustainable system. By combining the active sites of the metal with the controlled inner cavities formed by MOFs, metals and oxide - based nanoparticles may be incorporated into MOF materials to create Metal/MOFs with high heterogeneous catalysis performance. The use of MOFs as visible light photocatalysts for dyes removal and heavy metal ion removal is a novel field. ZIF-67 derivatives can also be employed as photocatalysts when exposed to visible light [46].

### 1.4.2.2 ZIFs for Electrochemistry

### 1.4.2.2.1 Electro-catalysis

ZIF-67 could also be used for preparing nanosheets which presented outstanding ability for the ORR, MOR, and HER owing to its increased current density, lower over-potential, aptitude for methanol tolerance, and enhanced stability[51].

## 1.5 Methanol Oxidation Reaction

The efficiency of the MOR utilized in DMFCs has a significant impact on their performance[52]. Methanol is catalytically oxidized to yield hydrogen ion and $CO_2$, which may be represented as[53]

$$CH_3OH + H_2O \rightarrow CO_2 + 6H^+ + 6e^- \quad E_o = 0.02V$$
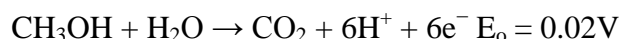
The proposed mechanism for MOR process is given in Figure 1.6.

Platinum and Pt-based catalysts are the most prevalent electrocatalysts for the methanol electrooxidation process at the moment (MOR). However, Pt-based catalysts have a number of drawbacks, including a high cost, a significant risk of CO poisoning, and still sluggish methanol electrooxidation kinetics, all of which limit their practical use in DMFCs. As a result, developing low-cost electrocatalysts with dramatically enhanced kinetics for MOR is critical [54].

Figure 0.6  Proposed mechanism of methanol oxidation reaction
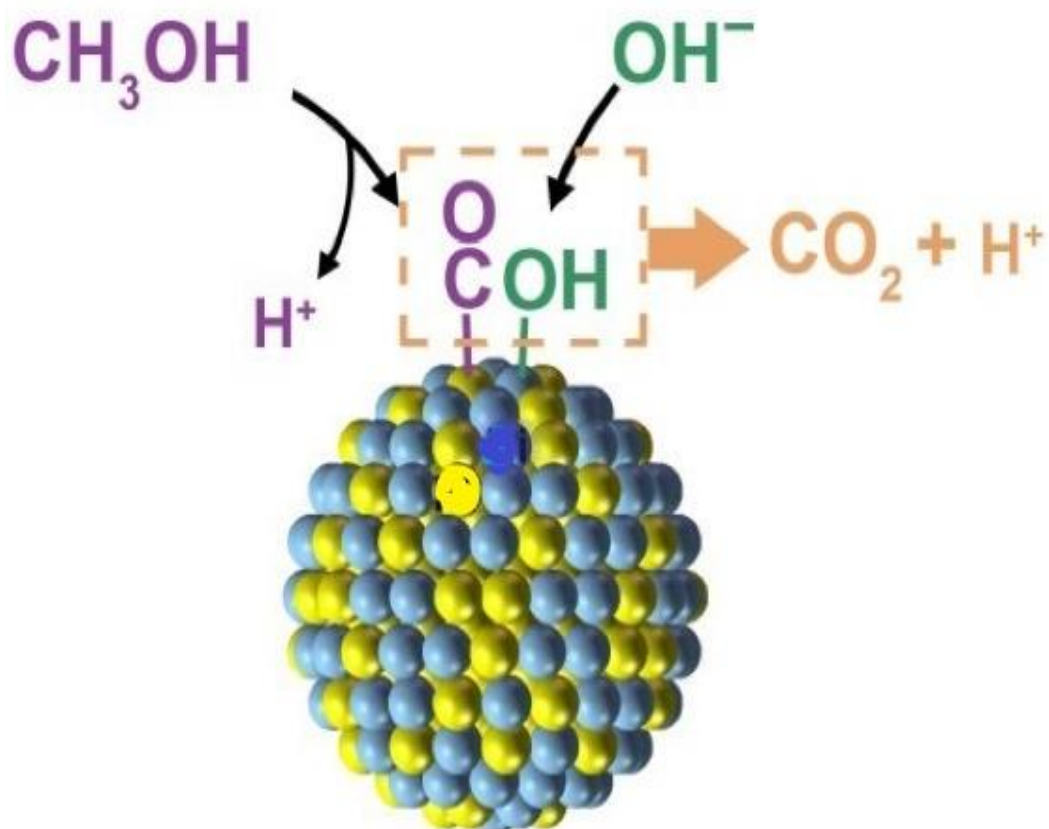


Figure 0.7 illustrative diagram of methanol oxidation reaction

**1.5.1 Electrocatalyst for Methanol Oxidation Reaction**

DMFCs have gained appeal as an effective power device. The sluggish kinetics of methanol oxidation and oxidation reduction processes are the primary barrier to further commercialization of DMFC (MOR and ORR). It employs the same Platinum catalyst as a PEMFC because it is a subtype of PEMFC. Pt, on the other hand, is a noble metal that may be poisoned by catalysis. As a result, a non-noble catalyst with anti-poisoning properties and the ability to quickly oxidize methanol is greatly desired. In this scenario, researchers have considered using non-precious transition metals (such as Co, Fe, Cu, and Ni) to improve catalyst performance. Transition metals (oxides and phosphides) were previously utilized as promotors. Surface engineering techniques such as metal-support interaction, surface doping, and core-shell structure have been developed to improve the performance of platinum catalysts. Pt-Ru is currently thought to be the finest performing catalyst[55].

- Because of the particular surface area of rGO and its electrical conductivity, the usage of $CeO_2$/rGO as an electro-catalyst displays greater activity toward methanol oxidation than $CeO_2$[56].

- The $Ni_{97}Bi_3$ aerogel electrocatalyst has a large number of active sites, efficient electron and mass transport, tolerance to CO poisoning, and excellent methanol oxidation performance[57].

- Other DMFC electrocatalysts include transition metal or nonprecious alloys. Many transition metals, including Ni, Cu, Mn, Co, and Fe, have been synthesized and employed in MOR reactions in the past; the most well-known of these are Ni and Fe nanostructures. These elements have attracted the interest of researchers owing to their low cost and catalytic activity under certain conditions such as electrocatalysis, hydrogenation, reformation, partial oxidation , and breakdown[58].

The problem statement of this research is the use of Platinum which is expensive and rare metal as an electrocatalyst for MOR. Catalyst poisoning because of the formation of intermediate CO that cause the poisoning of the catalyst. Loss of efficiency due to slow kinetics is also one of the problem that appears in MOR.

## 1.6 Research objectives

This research is based on the following objectives:

1. Synthesis of mono-metallic Co/NPC, bi-metallic MnCo/NPC, and ternary NiMnCo/NPC.

2. Characterization of the as prepared composite by using XRD, SEM/EDS, TEM, FT-IR, and XPS.

3. Electrochemical performance of the electro-catalyst using Cyclic voltammetry, Electrochemical impedance spectroscopy, and Chronoamperometry.

## Summary

This chapter discuss the background of fuel cells as an energy storage system and the methanol oxidation reaction in fuel calls in high energy density applications. Chapter 1 discusses the types and working of different fuel cells and their performance parameters in detail. Further challenges associated with DMFC is discussed in detail and possible mitigated techniques are mentioned.

# References

[1]     S. Newman, *The final energy crisis*. Pluto Press (UK), 2008.

[2]     M. S. Javed *et al.*, "The energy crisis in Pakistan: A possible solution via biomass-based waste," vol. 8, no. 4, p. 043102, 2016.

[3]     S. Shafiee and E. Topal, "When will fossil fuel reserves be diminished?," *Energy Policy,* vol. 37, no. 1, pp. 181-189, 2009/01/01/ 2009.

[4]     M. Tanzer, "Energy crisis: world struggle for power and wealth," 1974.

[5]     J.-M. Chevalier, "The new energy crisis," in *The New Energy Crisis*: Springer, 2009, pp. 6-59.

[6]     E. D. Coyle and R. A. Simmons, *Understanding the global energy crisis*. Purdue University Press, 2014.

[7]     D. E. Newton, *World energy crisis: a reference handbook*. Abc-clio, 2013.

[8]     L. Carrette, K. A. Friedrich, and U. J. C. Stimming, "Fuel cells: principles, types, fuels, and applications," vol. 1, no. 4, pp. 162-193, 2000.

[9]     E. Reddington *et al.*, "Combinatorial electrochemistry: a highly parallel, optical screening method for discovery of better electrocatalysts," vol. 280, no. 5370, pp. 1735-1737, 1998.

[10]    J. Cruickshank and K. J. J. o. P. S. Scott, "The degree and effect of methanol crossover in the direct methanol fuel cell," vol. 70, no. 1, pp. 40-47, 1998.

[11]    L. J. Blomen and M. N. Mugerwa, *Fuel cell systems*. Springer Science & Business Media, 2013.

[12]    C. Coutanceau, L. Demarconnay, C. Lamy, and J.-M. Léger, "Development of electrocatalysts for solid alkaline fuel cell (SAFC)," *Journal of Power Sources,* vol. 156, no. 1, pp. 14-19, 2006.

[13]    Y. Wang, K. S. Chen, J. Mishler, S. C. Cho, and X. C. Adroher, "A review of polymer electrolyte membrane fuel cells: Technology, applications, and needs on fundamental research," *Applied energy,* vol. 88, no. 4, pp. 981-1007, 2011.

[14]    Z. Zhan *et al.*, "Experimental study on different preheating methods for the cold-start of PEMFC stacks," *Energy,* vol. 162, pp. 1029-1040, 2018.

[15]    S. Gottesfeld and T. A. Zawodzinski, "Polymer electrolyte fuel cells," *Advances in electrochemical science and engineering,* vol. 5, pp. 195-302, 1997.

[16]    Z. Zhan *et al.*, "Experimental study on different preheating methods for the cold-start of PEMFC stacks," vol. 162, pp. 1029-1040, 2018.

[17]    Y. Lu, Y. Cai, L. Souamy, X. Song, L. Zhang, and J. Wang, "Solid oxide fuel cell technology for sustainable development in China: An over-view," *International Journal of Hydrogen Energy,* vol. 43, no. 28, pp. 12870-12891, 2018.

[18]    H. Lee, S. W. Yoon, E. J. Kim, and J. Park, "In-situ growth of copper sulfide nanocrystals on multiwalled carbon nanotubes and their application as novel solar cell and amperometric glucose sensor materials," *Nano Letters,* vol. 7, no. 3, pp. 778-784, 2007.

[19]    A. L. Dicks, "Molten carbonate fuel cells," *Current Opinion in Solid State and Materials Science,* vol. 8, no. 5, pp. 379-383, 2004.

[20]    K. Matsuoka, Y. Sato, and K. Kawano, "Direct methanol fuel cell system," ed: Google Patents, 2004.

[21]    Y. Muramatsu, H. Kohda, and S. Shiozawa, "Direct methanol fuel cell system," ed: Google Patents, 2006.

[22]    A. Faghri, Z. J. I. J. o. H. Guo, and M. Transfer, "Challenges and opportunities of thermal management issues related to fuel cell technology and modeling," vol. 48, no. 19-20, pp. 3891-3920, 2005.

[23]    S. R. Batten *et al.*, "Terminology of metal–organic frameworks and coordination polymers (IUPAC Recommendations 2013) %J Pure and Applied Chemistry," vol. 85, no. 8, pp. 1715-1724, 2013.

[24]    M. X. Wu and Y. W. J. A. M. Yang, "Metal–organic framework (MOF)- based drug/cargo delivery and cancer therapy," vol. 29, no. 23, p. 1606134, 2017.

[25]    K. M. Thomas, "Adsorption and desorption of hydrogen on metal–organic framework materials for storage applications: comparison with other nanoporous materials," *Dalton Transactions,* 10.1039/B815583F no. 9, pp. 1487-1505, 2009.

[26]    N. Stock and S. J. C. r. Biswas, "Synthesis of metal-organic frameworks (MOFs): routes to various MOF topologies, morphologies, and composites," vol. 112, no. 2, pp. 933-969, 2012.

[27]    J. Kim, S. Yeo, J.-D. Jeon, and S.-Y. Kwak, "Enhancement of hydrogen storage capacity and hydrostability of metal–organic frameworks (MOFs) with surface-loaded

platinum nanoparticles and carbon black," *Microporous and Mesoporous Materials,* vol. 202, pp. 8-15, 2015/01/15/ 2015.

[28]    B. Liu, H. Shioyama, T. Akita, and Q. Xu, "Metal-organic framework as a template for porous carbon synthesis," *Journal of the American Chemical Society,* vol. 130, no. 16, pp. 5390-5391, 2008.

[29]    N. A. Khan, Z. Hasan, and S. H. J. J. o. h. m. Jhung, "Adsorptive removal of hazardous materials using metal-organic frameworks (MOFs): a review," vol. 244, pp. 444-456, 2013.

[30]    M. Alhamami, H. Doan, and C.-H. J. M. Cheng, "A review on breathing behaviors of metal-organic-frameworks (MOFs) for gas adsorption," vol. 7, no. 4, pp. 3198-3250, 2014.

[31]    N. Rangnekar, N. Mittal, B. Elyassi, J. Caro, and M. J. C. S. R. Tsapatsis, "Zeolite membranes–a review and comparison with MOFs," vol. 44, no. 20, pp. 7128-7154, 2015.

[32]    H. Li, M. Eddaoudi, M. O'Keeffe, and O. M. Yaghi, "Design and synthesis of an exceptionally stable and highly porous metal-organic framework," *nature,* vol. 402, no. 6759, p. 276, 1999.

[33]    T. Xiao and D. J. M. T. E. Liu, "Progress in the synthesis, properties and applications of ZIF-7 and its derivatives," vol. 14, p. 100357, 2019.

[34]    C. Dey, T. Kundu, B. P. Biswal, A. Mallick, and R. Banerjee, "Crystalline metal-organic frameworks (MOFs): synthesis, structure and function," *Acta Crystallographica Section B: Structural Science, Crystal Engineering and Materials,* vol. 70, no. 1, pp. 3-10, 2014.

[35]    C.-C. Wang and J. Y. Ying, "Sol− gel synthesis and hydrothermal processing of anatase and rutile titania nanocrystals," *Chemistry of materials,* vol. 11, no. 11, pp. 3113-3120, 1999.

[36]    W. Liang and D. M. D'Alessandro, "Microwave-assisted solvothermal synthesis of zirconium oxide based metal–organic frameworks," *Chemical Communications,* vol. 49, no. 35, pp. 3706-3708, 2013.

[37]     W. Liang, R. Babarao, and D. M. D'Alessandro, "Microwave-Assisted Solvothermal Synthesis and Optical Properties of Tagged MIL-140A Metal–Organic Frameworks," *Inorganic chemistry,* vol. 52, no. 22, pp. 12878-12880, 2013.

[38]     A. Martinez Joaristi, J. Juan-Alcañiz, P. Serra-Crespo, F. Kapteijn, and J. Gascon, "Electrochemical synthesis of some archetypical Zn2+, Cu2+, and Al3+ metal organic frameworks," *Crystal Growth & Design,* vol. 12, no. 7, pp. 3489-3498, 2012.

[39]     P. J. Beldon, L. Fábián, R. S. Stein, A. Thirumurugan, A. K. Cheetham, and T. Friščić, "Rapid room- temperature synthesis of zeolitic imidazolate frameworks by using mechanochemistry," *Angewandte Chemie International Edition,* vol. 49, no. 50, pp. 9640-9643, 2010.

[40]     S. L. James *et al.*, "Mechanochemistry: opportunities for new and cleaner synthesis," *Chemical Society Reviews,* vol. 41, no. 1, pp. 413-447, 2012.

[41]     T. Friščić *et al.*, "Real-time and in situ monitoring of mechanochemical milling reactions," *Nature chemistry,* vol. 5, no. 1, p. 66, 2013.

[42]     N. Arul Dhas and A. Gedanken, "A sonochemical approach to the surface synthesis of cadmium sulfide nanoparticles on submicron silica," *Applied physics letters,* vol. 72, no. 20, pp. 2514-2516, 1998.

[43]     C. P. Raj, N. A. Dhas, M. Cherkinski, A. Gedanken, and S. Braverman, "Sonochemical synthesis of norbornane derivatives using allene cyclopentadiene Diels-Alder cycloaddition," *Tetrahedron letters,* vol. 39, no. 30, pp. 5413-5416, 1998.

[44]     C. Duan, Y. Yu, and H. Hu, "Recent progress on synthesis of ZIF-67-based materials and their application to heterogeneous catalysis," *Green Energy & Environment,* vol. 7, no. 1, pp. 3-15, 2022/02/01/ 2022.

[45]     C.-H. Kuo *et al.*, "Yolk–shell nanocrystal@ ZIF-8 nanostructures for gas-phase heterogeneous catalysis with selectivity control," vol. 134, no. 35, pp. 14345-14348, 2012.

[46]     R. Chandra, S. Mukhopadhyay, and M. J. M. L. Nath, "TiO2@ ZIF-8: A novel approach of modifying micro-environment for enhanced photo-catalytic dye degradation and high usability of TiO2 nanoparticles," vol. 164, pp. 571-574, 2016.

[47]     D. Matatagui *et al.*, "Chemoresistive gas sensor based on ZIF-8/ZIF-67 nanocrystals," vol. 274, pp. 601-608, 2018.

[48]    G. Zhong, D. Liu, and J. J. J. o. M. C. A. Zhang, "The application of ZIF-67 and its derivatives: adsorption, separation, electrochemistry and catalysts," vol. 6, no. 5, pp. 1887-1899, 2018.

[49]    Y. Han *et al.*, "A novel anode material derived from organic-coated ZIF-8 nanocomposites with high performance in lithium ion batteries," vol. 50, no. 59, pp. 8057-8060, 2014.

[50]    R. R. Salunkhe *et al.*, "A high-performance supercapacitor cell based on ZIF-8-derived nanoporous carbon using an organic electrolyte," vol. 52, no. 26, pp. 4764-4767, 2016.

[51]    B. Li *et al.*, "String of pyrolyzed ZIF-67 particles on carbon fibers for high-performance electrocatalysis," vol. 25, pp. 137-144, 2020.

[52]    L. Fan, Z. Tu, and S. H. Chan, "Recent development of hydrogen and fuel cell technologies: A review," *Energy Reports,* vol. 7, pp. 8421-8446, 2021/11/01/ 2021.

[53]    K. Ramya and K. J. J. o. E. C. Dhathathreyan, "Direct methanol fuel cells: determination of fuel crossover in a polymer electrolyte membrane," vol. 542, pp. 109-115, 2003.

[54]    S. J. Hoseini, M. Bahrami, and S. M. J. N. J. o. C. Nabavizadeh, "ZIF-8 nanoparticles thin film at an oil–water interface as an electrocatalyst for the methanol oxidation reaction without the application of noble metals," vol. 43, no. 39, pp. 15811-15822, 2019.

[55]    W. Chrzanowski and A. J. L. Wieckowski, "Surface structure effects in platinum/ruthenium methanol oxidation electrocatalysis," vol. 14, no. 8, pp. 1967-1970, 1998.

[56]    T. Han and Z. J. M. L. Zhang, "Novel hydrolyzing synthesis of CeO2–RGO support for Pt electrocatalyst in direct methanol fuel cells," vol. 154, pp. 177-179, 2015.

[57]    A. A. Dubale *et al.*, "High- Performance Bismuth- Doped Nickel Aerogel Electrocatalyst for the Methanol Oxidation Reaction," vol. 132, no. 33, pp. 13995-14003, 2020.

[58]    E. Antolini, J. R. Salgado, and E. R. J. A. C. B. E. Gonzalez, "The methanol oxidation reaction on platinum alloys with the first row transition metals: the case of Pt–

Co and–Ni alloy electrocatalysts for DMFCs: a short review," vol. 63, no. 1-2, pp. 137-149, 2006.

# Chapter 2:

# Literature Review

## 2.1 Direct Methanol Fuel Cells

Direct methanol fuel cells (DMFCs) have aroused a lot of attention due to their low operating temperature and excellent energy conversion efficiency. DMFCs are appealing energy technologies because of the ability of methanol to serve as a fuel storage medium under ambient circumstances, and the simplicity of deployment of such fuel cells. The effectiveness of the methanol oxidation process (MOR) utilized in DMFCs have significant effect on their performance[1]. Pd or Pt noble metals, are widely known as effective electro-catalysts for a variety of reactions. The methanol oxidation process using metal catalysts is both feasible and appealing. Pt alloying with less expensive metals (Co, Cu, Ni, and Fe) is a good way to increase activity and stability by adjusting the electrical and geometric heterostructures.

## 2.2 Platinum based Electro-catalyst for DMFC

S. S. Mahapatra et al. revealed the electrochemical production of a Pt-Pd/C catalyst with good efficiency in basic medium methanol oxidation. They investigated various methanol concentrations on a Pt-Pd/C catalyst and discovered that as methanol concentration increased, so did the peak current density. Until 1.0 M methanol concentration, there was a significant rise in peak current density. Because a linear rise in J value was seen with increasing NaOH concentration, the optimal MeOH/OH- ratio was reported as 1:2. For methanol and NaOH, the reaction orders are 0.45 and 0.70, respectively. Rct (2.38) and a low Tafel slop value indicate that PtPd/C is a viable catalyst for use in basic medium DMFCs[2]. Y. Li and colleagues developed a straightforward method for distributing Pt nanoparticles on graphene composites. The catalyst has superior stability and a current density of 199.6 mA/mg at a potential of 0.652 V, which is twice as much as the Pt-vulcan catalyst, which has a current density of 101.2 mA/mg at a potential of 0.664 V, indicating it to be a viable catalyst for methanol oxidation in DMFCs[3]. Y. Huang et al. described the creation of Pt nanoparticles by a

two-step rapid microwave aided polyol method in which they convert Pb+2 ions into Pb atoms for alloy formation with Pt at high temperatures using microwave. They analyze the created catalyst using XRD and TEM, which demonstrate that a core shell of Pt@PtPb catalyst was generated at the conclusion of the process when the Pb+2 ions were exhausted. The core was a platinum nanoparticle, while the shell was comprised entirely of Pt-Pb alloyed nanoparticles. The average diameter of the catalysts was 5.9 nm[4]. M. Ku Jeon et al. presented a Pt/WC catalyst and examined its structural and electrochemical properties. When compared to Pt/C catalyst, Pt/WC has a lower peak potential (0.68 V). The presence of Ru in the catalyst has a little effect on particle size, with an average particle size of around 2-3 nm for 3:1 and 1:1 Pt: Ru catalysts, which is comparable to the crystallite size of Pt particulate supported on the same substrate. For 90 percent particles, the particle size distribution Pt:Ru by HREM was 0.5 nm for 3:1 and 0.2 nm for 1:1. Second, while the particles were found to have a homogenous composition, they were unable to detect the presence of surface segregation in the individual crystals, if any existed. Third, the existence of (111) and (200) crystallographic planes, as seen in pure Pt and many fcc metal nanocrystals, causes the majority of particles to be cubic octahedral in form. Sporadic (113) forms of facets were also identified, which are not fcc type nanocrystals and do not appear in the case of pure pt particles on the same support. This paper demonstrates how long scientists have struggled to discover the truth underlying the methanol oxidation reaction, as well as the major importance of electrochemical catalysts needed for methanol oxidation[5]. X. Ma et al. proposed in situ formation of Cu-Ni metal nanoparticles comprises of a bimetallic MOF created by etching two non-noble metal component nanoparticles for OER. The encapsulating of metal nanoparticles increases the conductivity and stability of MOF while also providing active metal sites for increased activity of the oxygen evolution process. Due to the synergistic effect, this bimetallic system outperforms monometallic systems in terms of efficiency[6].

## 2.3 Transition metals and alloys based electrocatalyst for DMFC

Different metals and alloys were also used as an electro-catalyst for methanol oxidation reaction (MOR), H. Huang et al. discovered a simple and straightforward technique for the more efficient synthesis of MWCNT supported Pt/CoPt composite NPs using

solution plasma sputtering followed by thermal annealing. With mass activities of 1719mA mg1 Pt, the derived Pt/CoPt/MWCNTs composite catalysts significantly improved methanol electro-oxidation in acidic environments. Because of the multiple active sites and smooth surface of the catalysts, this value is substantially greater than that reported before for Pt-Co alloy [7]. E. Antolini studied the electrochemical oxidation of methanol on Pt/Co and Nickel alloy electrocatalysts. When the base metal concentration is low, the onset potential for the MOR increases with increasing Co/Ni quantity in the catalyst, however when the base metal content is large, the onset potential for the MOR decreases with increasing Co/Ni. The degree of alloying, in addition to the base metal concentration, plays a crucial impact in the MOR activity of these catalysts[8]. Jian Lan et al. revealed trimetallic PtNiCu nanoalloys for methanol oxidation, demonstrating that a small amount of Ni added to PtCu alloys can improve MOR efficiency and stability. Their findings demonstrate that Ni-doped PtCu nanoalloys are effective electrocatalysts for DMFC in acidic media. $Pt_{60}Ni_3Cu_{37}$ has the best catalytic performance and a 12% mass loss as measured by Chronoamperometry, while $Pt_{60}Ni_{13}Cu_{27}$ has a 27% mass loss and is less efficient than the previous one. Furthermore, standard Pt black and porous $Pt_{55}Cu_{45}$ were compared to $Pt_{60}Ni_3Cu_{37}$, which was shown to be less efficient[9].

## 2.4 Metal-oxide based electrocatalyst for DMFC

Various metal based metal oxides were also reported as electro-catalyst for the MOR. I. Danaee et al. reported the electrochemical deposition of NiO films on Ni and Ni-Cu alloy on GCE and evaluated for impedance investigations of electrochemical MOR in basic media. Two semicircles showed positive resistance for GC/Ni after Rct and intermediate adsorption, while impedance plots of GC/NiCu showed negative resistance. Impedance data was evaluated at various potentials, revealing the presence of two simultaneous processes at the interface: intermediate generation as a result of methanol oxidation and oxidation of those intermediates. Variable potential also revealed changes in the process and rate-determining step. Meanwhile, r.d.s of MOR intermediate potential were found in the transition range[10]. Z.K. Ghouri et al demonstrated 4nm sized submicron $ZnO/CeO_2$ dots@CNFs with strong dispersion on the surface of CNFs and this dispersion boosted its methanol activity, making it a competitive and non-

precious choice for DMFCs application. They manufactured these nanodots in two ratios, with peak current densities of 5.3 mA/cm$^2$ and 16.3 mA/cm$^2$ at a scan rate of 50mV/s, respectively. K.C[11]. Devarayapalli et al. used a quick microwave synthesis approach to create nanocomposites of ZIF-8 generated ZnO and ZnO@Ta$_2$O$_5$ (Ta$_2$O$_5$ attached to ZIF-8 produced ZnO). XRD, XPS, BET, SEM, and HR-TEM were used to analyze the ZIF-8, ZnO, and ZnO@Ta$_2$O$_5$ that were synthesized. According to our findings, the ZnO@Ta$_2$O$_5$ electrode performed admirably in these reactions in terms of activity and stability[12].

## 2.5 MOFs based electro-catalyst for DMFC

MOFs arise as a group of compound with unusual characteristics like ultrahigh porosity with free volume up to 90% and high internal surface area. One of the hallmarks of MOFs is their esthetically pleasing structures and topologically diverse nature. Many of them use minerals as precursors for designing a structure with desirable properties and functions that shows the eternal aspiration of scientist. The contrast of two elements of MOFs include metal ion and the organic linker which bear endless possibilities for combination resultantly provide various properties due to the summation of inorganic and organic components. R. Mehak et al. revealed the hydrothermal synthesis of Co-MOF-71 and its blends with rGO. They also use FTIR, XRD, SEM, and XPS to characterize their manufactured materials. They investigated the chemical activity of MOR catalysts using three electrode systems: a working modified glassy carbon GCE electrode, a reference Ag/AgCl electrode, and a counter Pt wire electrode in basic media of 1M NaOH + 3M CH$_3$OH. At potential 0.1V, a considerable peak current density (29.1mA/cm$^{-2}$) was recorded. These findings indicate that it is a viable material for MOR fuel cell applications[13]. Using organic linkers such as pyrazine and 2,5-dihydroxyterephthalic acid, T. Noor et.al, reported a novel bi-metallic (MOF), nickel oxide, and ferrous oxide catalyst was produced. Its composites were created in collaboration with reduced graphene oxide to promote electrochemical processes with bi-metallic MOF (rGO). Physical characteristics were assessed using SEM, EDX, XRD, FTIR, Raman spectroscopy, TGA, and BET analysis. The Ni-Fe composites were subjected to electrochemical tests of cyclic voltammetry (CV) in a 3M methanol solution. At 50 mV/sec and 0.9 V, the composite has a promising current density of

437.28 mA/cm$^2$. L. Yaqoob et al. used solvothermal techniques to create Ni-BTC MOF and composites of different ratios of rGO. For physical characteristics, SEM, EDX, XRD, and FTIR analyses were performed. As the working electrode, a modified glassy carbon electrode was employed. Methanol oxidation processes were carried out in a 2M methanol solution with a support electrolyte of 1M NaOH. The greatest results were obtained with Ni-BTC/4wt percent rGO of about 200.22 mA/cm2 at 0.69 V and 50 mV/sec. The current density steadily increases as the amount of catalyst increases until it reaches 2 mg, which was identified as the appropriate concentration for further treatments[14].

Due to numerous possible combinations, a number of metal organic frameworks has been reported which can be customized according to the applications for which they are used. So, the metals and organic linkers present in metal organic framework should in accordance with the applications that need to be performed. By keeping in mind this point we can even get good efficiency and performance by these MOFs. H. Ramezanalizadeh et al. presented the simple synthesis of unique BiFeO$_3$ on the Co/Ni MOF composite, that is magnetic, durable, and highly efficient photocatalyst, and confirmed their synthesis by SEM, XRD, FTIR, DRS, VSM, BET, EDX, and TEM. They also take note of various experimental parameters. Using placid circumstances, the results indicated that BiFeO$_3$ (1:1) proved to be a very effective photocatalyst for the breakdown of MO and 4-NP pollutants. When magnetic BiFeO$_3$ is immobilized on Co/Ni-MOF, the catalyst's activity improves in all areas. T. Noor et al. reported the production of Cu-MOFs and their graphene oxide composites with varying graphene oxide weight percentages (GO). The constructed 3D metal organic framework has significant MOR electrocatalytic activity. Among all produced catalysts, 5wt% GO/Cu-MOF exhibits the greatest activity, with peak current density of 10mA/cm$^2$ at 0.8V potential. This catalyst's current density is comparable to that of commercially available Pt/C catalysts, however stability must be increased by additional modification. Because of the equivalent results with Pt-based catalysts, it can be used as a cost-effective alternative to pricey catalysts in DMFC with commercial viability[15]. A. Abbasi et al. The utilization of moderate conditions resulted in the synthesis of a mixed Co/Ni MOF using a hydrothermal technique to eliminate the hue of Bismarck brown. They also use

24

single crystal XRD to characterize produced material. Their synthesized MOF has high stability and efficiency for dye removal, and its separation from aqueous solution is simple, allowing it to be employed for at least three cycles[16]. M. S. Rahmanifar et al. produced Ni-MOF and Co-MOF as described previously technique within the same reaction vessel, as well as synthesis of Ni/Co-MOF-rGO nanocomposites by using the same approach with amazing super-capacitive performance with specific capacitance value of 850 F/g at 1 A/g [17]. X.Wang et al. presented the hydrothermal approach that was used to successfully construct NiCo-based MOFs, and structural characterization such as SEM, TEM, PXRD, FTIR, and TG analyses verified the coordination of Ni and Co ions with BPDC ligand. As one-dimensional micro-nanorods build three-dimensional regular cuboids, these characterizations reveal that MOFs have high crystallinity. Electrochemical studies on the capacitance of prepared MOFs revealed significant pseudo capacitive performance of 990.7 $Fg^{-1}$ (at $1Ag^{-1}$), excellent rate capacity supported by a capacity value of 405.0 $Fg^{-1}$ (at $20Ag^{-1}$), and excellent capacitance retention with a value of 553.2 F/g (at 1A/g) after 3000 cycles. All of the findings show that NiCo-MOF may be used as an electrode material in supercapacitors[18].

## 2.6 ZIFs as an electrocatalyst for DMFC

ZIFs (Zeolite Imidazole Framework) are MOFs consisted transition metal ions such as $Zn^{2+}$, $Co^{2+}$, $Fe^{2+}$, or $Cu^{2+}$ of four-coordinated and a linker of imidazolate ion. The two most frequently investigated ZIFs in the last several decades are ZIF-8 (Zn based) and ZIF-67 (Co based). Mostly at room temperature both of the Zifs can be easily produced, and the shapes and structures of these ZIFs may be customized utilizing a variety of mild solvothermal conditions. S.J. Hoesini. reported the first instance of a ZIF-8 nanostructured layer at the oil-water interface. In compared to membrane electrode assemblies/PtRu (6.8 mW $cm^{-2}$) anodes, the as-synthesized ZIF-8 film displayed a significant power quantity of 15.4 mW $cm^{-2}$[19]. X.Shi et al. The reported pyrolysis of ZIF-67 at $700^oC$ in an Ar/H2 atmosphere for the formation of Pt nanoparticles mounted on carbon nanotubes framework doped with nitrogen. RDE analysis reveals that Pt-Co@NCNTs outperform generally viable Pt/C electrocatalysts in perchloric acid for oxygen reduction reaction (ORR). CV analysis validated the stability of Pt-Co@NCNTs, which exhibit only a 6% depletion in J after 50 cycles, whereas commercial Pt/C

displays a 15% degradation under the same conditions. The MEA with Pt-Co@NCNTs demonstrated significantly higher PEMFC efficiency with a peak J value of 630 mWcm-2 compared to commercial Pt/C with a peak current density of 570 mWcm-2 while Pt loading was the same (0.12 mg cm-2) with the assistance of nafion-212[20]. X. L. Sui et al. described a new technique for creating a porous N-doped graphene aerogel with an open structure and numerous defects by hydrothermal self-assembly of ZIF-8 and GO. Furthermore, the addition of N and Zn results in an abundance of N-doped sites and a microporous structure. This study provides a viable strategy for synthesizing good N-doped carbon materials for electrochemical applications by employing ZIF-8 derivatives[21]. Y. Liu et al. investigated a bimetallic CoNi-zeolitic imidazole framework embedded by $MoS_2$ nanosheets ($MoS_2$@CoNi-ZIF) nanocomposite as a bifunctional electrocatalyst for non-Pt methanol oxidation process (MOR) and overall water splitting in an alkaline solution. The catalytic activity of the $MoS_2$@CoNi-ZIF nanocomposites vary. Significantly, the $MoS_2$@CoNi-ZIF nanosheet with a $MoS_2$: CoNi-ZIF ratio of 3: 1 ($MoS_2$@CoNiZIF(3-1)) exhibits exceptional electrocatalytic activity for MOR, with an oxidation potential of 1.6 V, as well as high catalytic current density and durability. Furthermore, the $MoS_2$@CoNiZIF(3-1) nanocomposite outperforms HER and OER electrocatalytically. This study identified a viable electrocatalyst for the development of high-performance non-Pt-based clean energy and fuel cells in alkaline solution[22]. F. He et al. described a unique method for fabricating a PtCo/NCS catalyst with bimetallic PtCo nanoparticles based on a NCS produced from an UA-ZIF-67 template. Pt and Co metallic NP are evenly supported on the NCS in the best PtCo/NCS. Because of its high ECSA, current density, steady-state current, and current retention, this PtCo/NCS catalyst exhibits significant electrocatalytic activity and stability for MOR. These insights gave fresh insight into the design and manufacturing processes[23].

## Summary

This chapter consists of the literature review on the types of electrocatalyst materials used for DMFC. The performance of different materials that are used as an electrocatalyst for MOR in DMFC is also discussed in the chapter. Moreover, this chapter also contains the benefits and shortcomings of MOF and ZIF derived materials for the energy storage applications.

# References

[1]     G. Tritsaris and J. J. T. J. o. P. C. C. Rossmeisl, "Methanol oxidation on model elemental and bimetallic transition metal surfaces," vol. 116, no. 22, pp. 11980-11986, 2012.

[2]     S. Mahapatra and J. Datta, "Characterization of Pt-Pd/C electrocatalyst for methanol oxidation in alkaline medium," *International Journal of Electrochemistry,* vol. 2011, 2011.

[3]     X. Xu, Y. Zhou, T. Yuan, and Y. J. E. A. Li, "Methanol electrocatalytic oxidation on Pt nanoparticles on nitrogen doped graphene prepared by the hydrothermal reaction of graphene oxide with urea," vol. 112, pp. 587-595, 2013.

[4]     Y. Huang, J. Cai, and Y. J. i. j. o. h. e. Guo, "Roles of Pb and MnOx in PtPb/MnOx-CNTs catalyst for methanol electro-oxidation," vol. 37, no. 2, pp. 1263-1271, 2012.

[5]     M. K. Jeon, K. R. Lee, W. S. Lee, H. Daimon, A. Nakahara, and S. I. J. J. o. P. S. Woo, "Investigation of Pt/WC/C catalyst for methanol electro-oxidation and oxygen electro-reduction," vol. 185, no. 2, pp. 927-931, 2008.

[6]     X. Ma, K. Qi, S. Wei, L. Zhang, X. J. J. o. A. Cui, and Compounds, "In situ encapsulated nickel-copper nanoparticles in metal-organic frameworks for oxygen evolution reaction," vol. 770, pp. 236-242, 2019.

[7]     H. Huang, X. Hu, J. Zhang, N. Su, and J. J. S. r. Cheng, "Facile fabrication of platinum-cobalt alloy nanoparticles with enhanced electrocatalytic activity for a methanol oxidation reaction," vol. 7, no. 1, pp. 1-9, 2017.

[8]     E. Antolini, J. R. Salgado, and E. R. J. A. C. B. E. Gonzalez, "The methanol oxidation reaction on platinum alloys with the first row transition metals: the case of Pt–Co and–Ni alloy electrocatalysts for DMFCs: a short review," vol. 63, no. 1-2, pp. 137-149, 2006.

[9]     J. Lan, C. Li, T. Liu, and Q. J. J. o. S. C. S. Yuan, "One-step synthesis of porous PtNiCu trimetallic nanoalloy with enhanced electrocatalytic performance toward methanol oxidation," vol. 23, no. 1, pp. 43-51, 2019.

[10] I. Danaee, M. Jafarian, F. Forouzandeh, F. Gobal, and M. J. I. J. o. H. E. Mahjani, "Electrocatalytic oxidation of methanol on Ni and NiCu alloy modified glassy carbon electrode," vol. 33, no. 16, pp. 4367-4376, 2008.

[11] Z. K. Ghouri *et al.*, "Nano-engineered ZnO/CeO2 dots@ CNFs for fuel cell application," *Arabian Journal of Chemistry,* vol. 9, no. 2, pp. 219-228, 2016.

[12] K. Devarayapalli, S. P. Vattikuti, K. S. Yoo, P. Nagajyothi, and J. J. J. o. E. C. Shim, "Rapid microwave-assisted construction of ZIF-8 derived ZnO and ZnO@ Ta2O5 nanocomposite as an efficient electrode for methanol and urea electro-oxidation," vol. 878, p. 114634, 2020.

[13] R. Mehek, N. Iqbal, T. Noor, H. Nasir, Y. Mehmood, and S. Ahmed, "Novel Co-MOF/Graphene Oxide Electrocatalyst for Methanol Oxidation," *Electrochimica Acta,* vol. 255, pp. 195-204, 2017/11/20/ 2017.

[14] T. Noor, M. Ammad, N. Zaman, N. Iqbal, L. Yaqoob, and H. Nasir, "A Highly Efficient and Stable Copper BTC Metal Organic Framework Derived Electrocatalyst for Oxidation of Methanol in DMFC Application," *Catalysis Letters,* pp. 1-16, 2019.

[15] H. Ramezanalizadeh and F. J. J. o. C. P. Manteghi, "Synthesis of a novel MOF/CuWO4 heterostructure for efficient photocatalytic degradation and removal of water pollutants," vol. 172, pp. 2655-2666, 2018.

[16] A. Abbasi, M. Soleimani, M. Najafi, and S. Geranmayeh, "New interpenetrated mixed (Co/Ni) metal–organic framework for dye removal under mild conditions," *Inorganica Chimica Acta,* vol. 439, pp. 18-23, 2016.

[17] M. S. Rahmanifar, H. Hesari, A. Noori, M. Y. Masoomi, A. Morsali, and M. F. J. E. A. Mousavi, "A dual Ni/Co-MOF-reduced graphene oxide nanocomposite as a high performance supercapacitor electrode material," vol. 275, pp. 76-86, 2018.

[18] W. Yang *et al.*, "Shapeable three-dimensional CMC aerogels decorated with Ni/Co-MOF for rapid and highly efficient tetracycline hydrochloride removal," vol. 375, p. 122076, 2019.

[19] S. J. Hoseini, M. Bahrami, and S. M. J. N. J. o. C. Nabavizadeh, "ZIF-8 nanoparticles thin film at an oil–water interface as an electrocatalyst for the

methanol oxidation reaction without the application of noble metals," vol. 43, no. 39, pp. 15811-15822, 2019.

[20] X. Shi, N. Iqbal, S. Kunwar, G. Wahab, H. Kasat, and A. M. J. i. j. o. h. e. Kannan, "PtCo@ NCNTs cathode catalyst using ZIF-67 for proton exchange membrane fuel cell," vol. 43, no. 6, pp. 3520-3526, 2018.

[21] X.-L. Sui, L.-M. Zhang, L. Zhao, D.-M. Gu, G.-S. Huang, and Z.-B. J. I. J. o. H. E. Wang, "Nitrogen-doped graphene aerogel with an open structure assisted by in-situ hydrothermal restructuring of ZIF-8 as excellent Pt catalyst support for methanol electro-oxidation," vol. 43, no. 48, pp. 21899-21907, 2018.

[22] B. Liu, H. Shioyama, T. Akita, and Q. Xu, "Metal-organic framework as a template for porous carbon synthesis," *Journal of the American Chemical Society,* vol. 130, no. 16, pp. 5390-5391, 2008.

[23] F. He *et al.*, "ZIF-8 derived carbon (C-ZIF) as a bifunctional electron acceptor and HER cocatalyst for gC 3 N 4: construction of a metal-free, all carbon-based photocatalytic system for efficient hydrogen evolution," vol. 4, no. 10, pp. 3822-3827, 2016.

# Chapter 3:

## Methodology and Characterization

### 3.1 Methodology

#### 3.1.1 Simple Solution Mixing

It is a simple synthesis technique in which all the precursors are dissolved in a liquid solution and then mechanically stir the solution by magnetic stirrer. This process is normally done at room temperature. As a result, the product is obtained in the form of precipitates. The product is then filtered or centrifuges, washed with the solvent such as methanol, ethanol or distilled water and then dried.

### 3.2 Characterization Techniques

#### 3.2.1 Fourier Transform infrared Spectroscopy (FTIR)

The term FTIR named as a "Fourier transform" is requisite to exchange the raw data into the actual processed spectrum. FTIR spectrophotometer using IR radiation having wavelengths longer than visible range gives a wide spectral range in the form of actual spectrum for specific functional groups or class of compounds [1].

FTIR is an indicative technique which gives the,identification,for the presence of a band the prepared sample. It concurrently collects the data in high,spectral-resolution,over,a wide spectral, range and relies on the fact that most of the absorbed light lies in infrared region of electromagnetic spectrum. Spectrophotometer produces an optical signal with all absorbed or emitted IR frequencies in it in the form of spectrum to evaluate the presence of different groups or classes in the examined compound. So two types of spectra can be obtained from this technique. The one which is obtained by absorption of IR radiation while the other due to transmitted IR radiation named absorption and transmission spectra respectively. [2].

The basic structure and working principle of FTIR instrument is shown below:
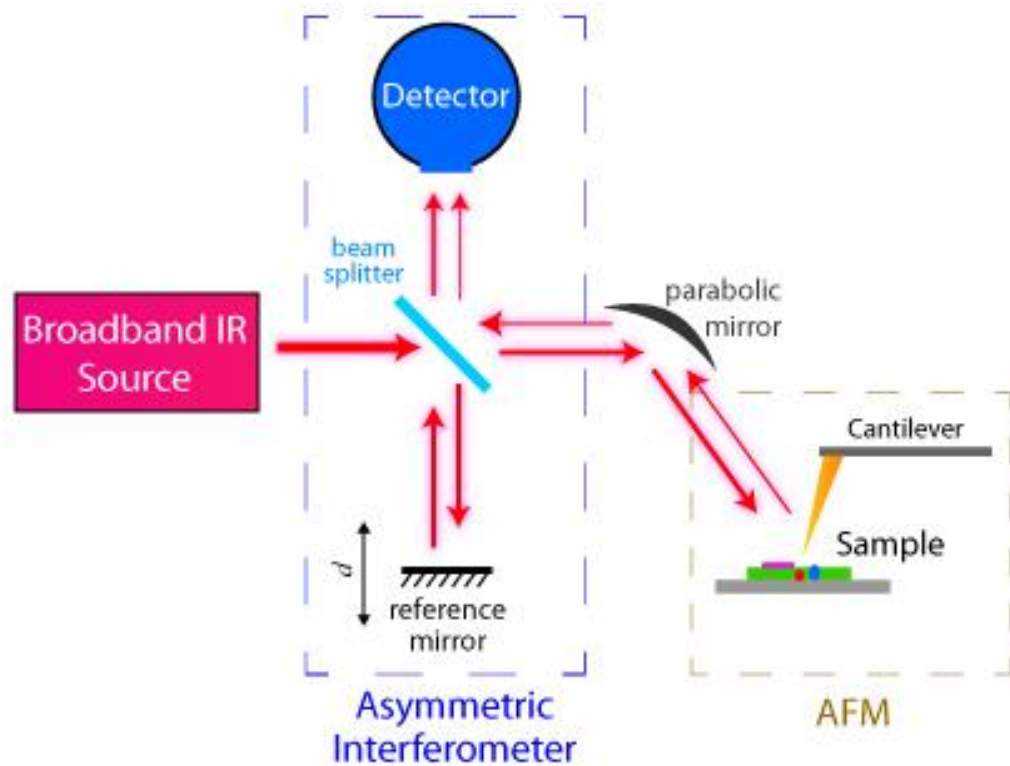
Figure 0.1 Working principle of FTIR Spectrometer

### 3.2.2 X-ray Diffraction ( XRD)

XRD is a brisk analytical technique usually served for recognition of phase and inquiring crystalinity of the material. According to Max von Laue, behavior of crystalline substances like 3D for gratings of wavelengths of X-ray which are closely related to the planes of crystal lattice [3]. The fundamental principle of XRD is relied on constructive interference of sample under examination with monochromatic X-rays. Cathode ray tube is used as a source of X-ray which is then filtered through monochromator for the production of monochromatic waves and then heading towards sample. XRD is a swift analytical technique which is utilized to identify phase of a sample and information about dimensions of a unit cell. The sample to be analyzed should be homogenized, grounded finely and average bulk composition [4].

Constructive interference (diffracted ray) is generated when incoming rays intermingle with that of sample under examination when conditions satisfy, Bragg's law i.e.

**$2d \sin\theta = n\lambda$**

Where;                                    **d**= interlayer distance

32

**n**= number of layer under consideration

ƛ= wavelength


XRD is intended so that best possible quality of diffraction data can be obtained. It comprise of three main elements (1) X-ray tube (2) sample holder and (3) X-ray detector [5]. An X-ray diffractometer bears a simple geometry in which the sample material rotate in the way of incident.
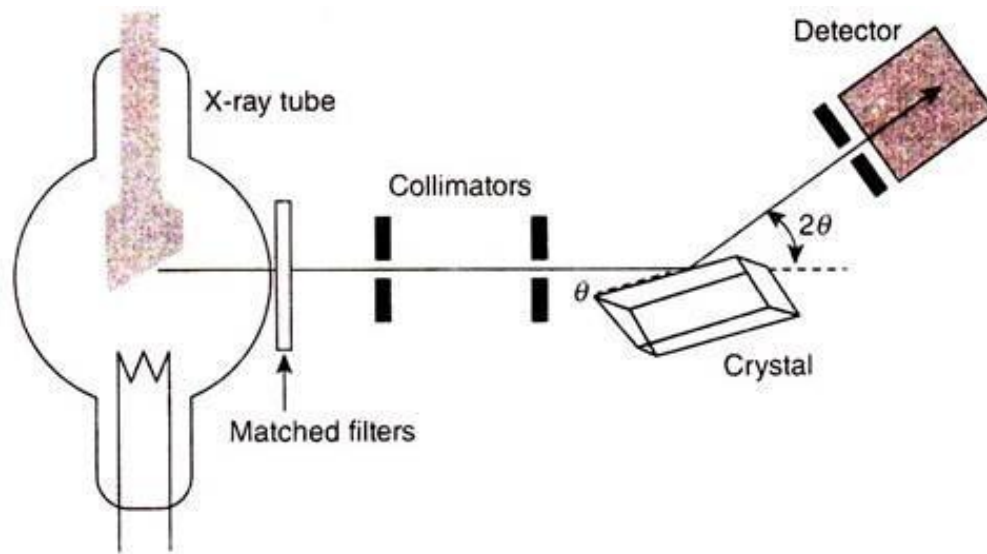


Figure 0.2 Workimg principle of XRD

### 3.2.3 Scanning Electron Microscopy (SEM)

SEM is utilized to scan a concentrated beam of electrons over a surface for interaction to form an image which shows the surface morphology of sample under examination and shape of crystals is used very effectively in microanalysis of the micro structures. These signals also bears secondary electron that form SEM images and also provide orientation of minerals and crystalline structure of material by backscattered electrons (BSE). X-rays which are utilized for elemental analysis, light of visible range and heat [6]. SEM analysis is said to be "non-destructive" as no volume loss has observed during X-rays generation by electrons interaction as electron do not penetrate into the sample and they made on surface interaction with the sample, which make it possible to analyze the material repeatedly [7].
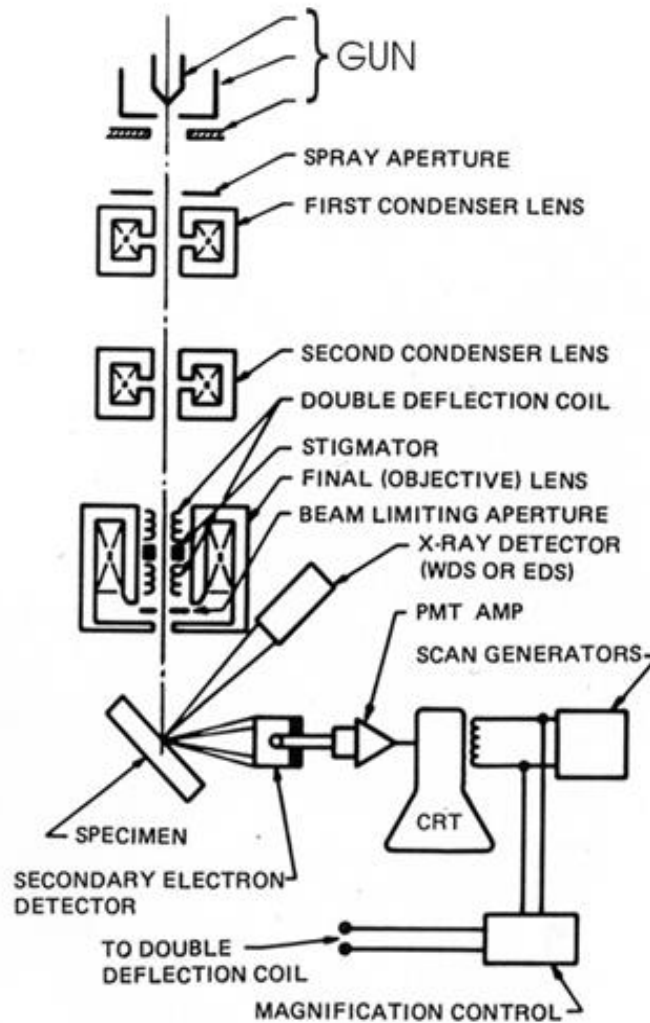
Figure 0.3 Workimg principle of SEM

Main elements of SEM are given in Figure 1.19. Scanning electron microscopy works rapidly as it completes BSE, SEI and EDS is less than five minutes. It gives us morphological, compositional and topological information. Detection of fractures can also be possible which give qualitative analysis of the material [8].

### 3.2.4 X-RAY Photoelectron Spectroscopy (XPS)

XPS is a quantitative spectroscopic (surface-sensitive) technique based on the photoelectric effect that can identify the elements that exist within a material (elemental composition) or that cover its surface, as well as their chemical state, overall electronic structure, and density of the electronic states in the material. XPS is a strong measuring

technique since it displays not only what elements are there, but also to what other elements they are linked[9].

The kinetic energy and quantity of ejected electrons are used to infer chemical states. High vacuum (residual gas pressure p 106 Pa) or ultra-high vacuum (p 107 Pa) conditions are required for XPS, while ambient-pressure XPS, in which samples are evaluated at pressures of a few tens of millibars, is a current field of investigation[10].
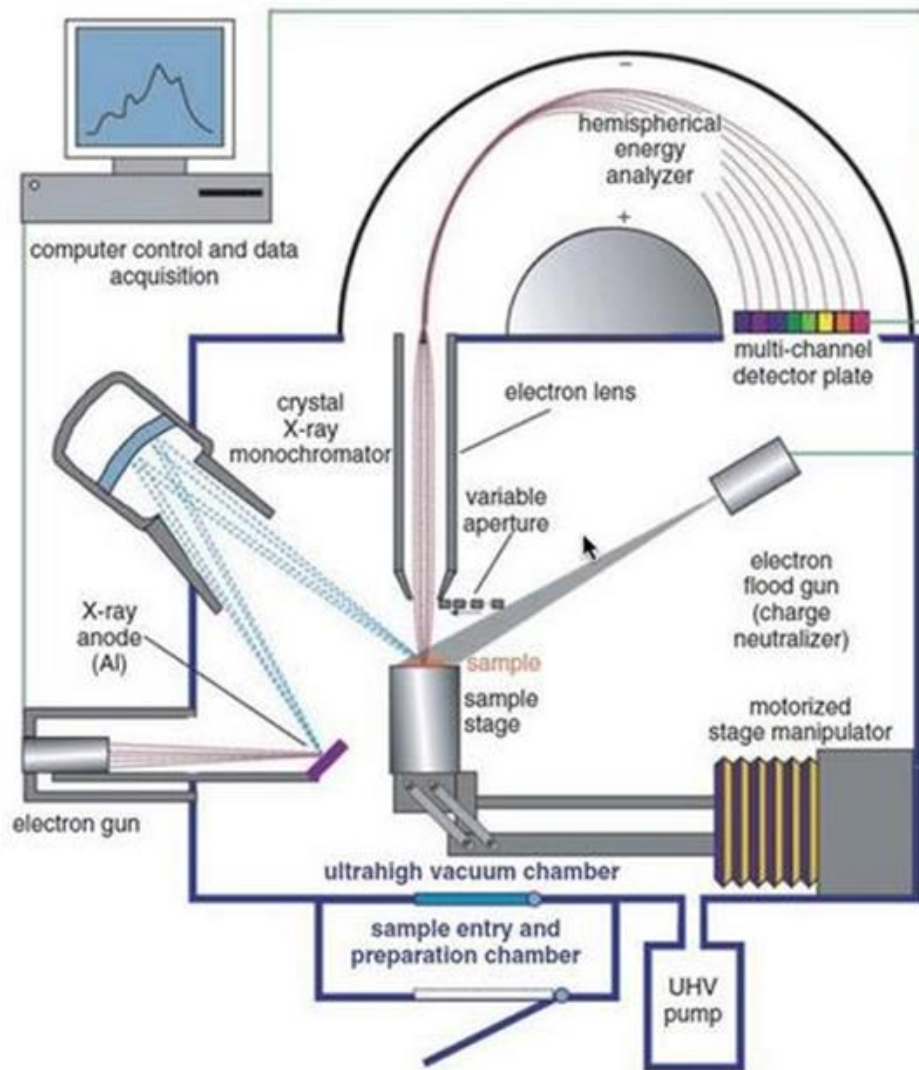


Figure 0.4 Workimg principle of XPS

Because it produces good quantitative precision from homogenous solid-state materials, XPS is often used to construct empirical formulas. Absolute quantification necessitates the use of certified (or independently validated) reference samples, is more difficult, and

is less prevalent. Comparing various samples in a set for which one or more analytes are altered but all other components (the sample matrix) remain constant is what relative quantification entails. Under ideal conditions, the atomic percent (at percent) values computed from the primary XPS peaks have a quantitative accuracy of 90-95 percent for each peak. Quantitative accuracy for lesser XPS signals with peak intensities 10-20% of the strongest signal is 60-80% of the real value, depending on the amount of effort needed to increase the signal-to-noise ratio (for example by signal averaging). For correct reporting of quantitative data, quantitative accuracy (the ability to repeat a measurement and receive the same result) is critical[11].

### 3.2.5 Transmission Electron Microscopy (TEM)

A beam of electrons is passed through a specimen to generate an image in transmission electron microscopy (TEM). A suspension on a grid or an ultrathin section less than 100 nm thick are the most common specimens. The interaction of the electrons with the sample as the beam passes through the specimen creates a picture. The picture is amplified and focused onto an imaging device, such as a fluorescent screen, a layer of photographic film, or a sensor linked to a charge-coupled device, such as a scintillator[12].
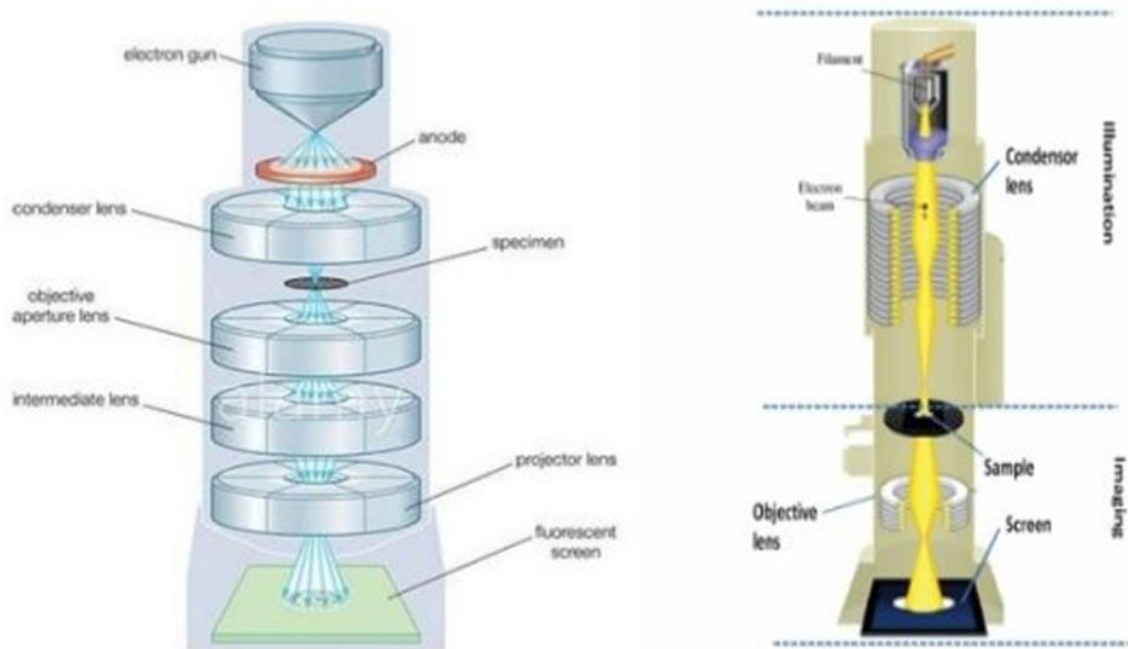


Figure 0.5 Workimg principle of TEM

The tool can record exquisite detail as tiny as a single column of atoms, which is thousands of times smaller than a resolvable object observed under a light microscope. In the physical, chemical, and biological sciences, transmission electron microscopy is a common analytical technique. TEM can produce a wide range of nanometer and atomic-resolution data, indicating not only where all the atoms are, but also what sorts of atoms they are and how they are connected to one another in perfect circumstances. As a result, TEM is considered a critical tool for nanoscience in both biological and materials disciplines[13].

## 3.3 Electrochemical Techniques

### 3.3.1 Cyclic Voltametery (CV)

One of the efficient methods for the examination of electrochemical reactions is cyclic voltammetry which measure the current develops in a electrochemical cell. Perhaps, it is the most adaptable electrochemical technique to study the efficiency of electroactive species.
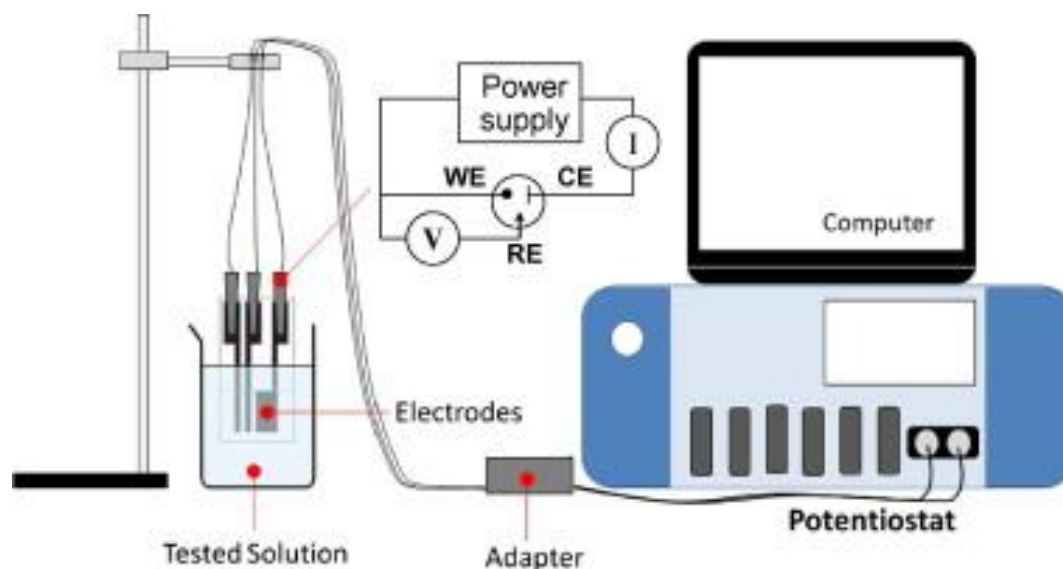


Figure 0.6 Measurement procedure by CV

Fundamental components of CV include potential of working electrode immersed in unstirred solution of electrolyte. Potential can be controlled against reference electrode for example, (Ag/AgCl). A cyclic voltammogram results by current measurement of the working electrode by applying potential. The voltammogram is a representation of

current against potential. As the potential changes with time, so it can take it as time axis which gives any easy understanding on the basics of this technique [14].
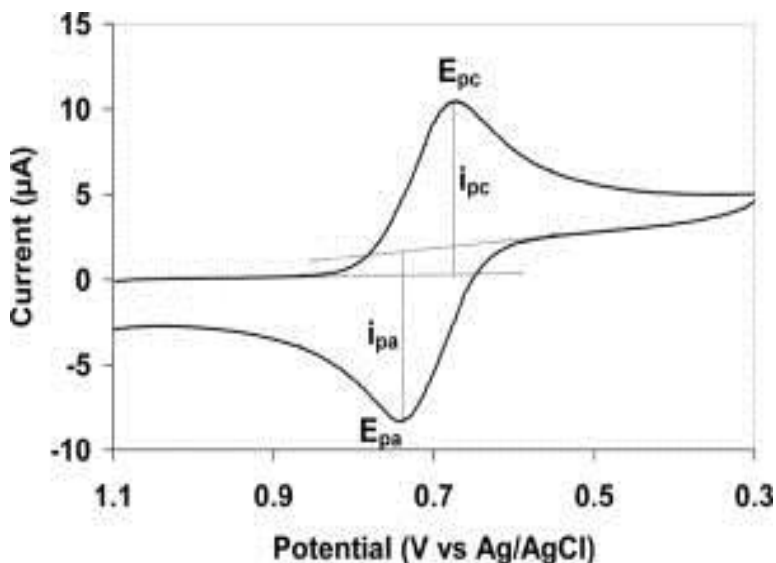


Figure 0.7 Cyclic voltamogram

It can be used to analyze kinetic path of the reaction where charge transfer reaction occur between electrodes influenced by electrode potential. In this technique, the reaction drives in forward reaction by giving a fixed potential to the working electrode in the meantime axillary electrode is capturing the electrons to complete the circuit. The applied potential is usually among working and reference electrodes while measurement of current took place between working and counter electrodes. Provided electrolyte gives conductivity among electrodes [15].

### 3.3.2 Electrochemical Impedance spectroscopy (EIS)

This is another useful technique which is gaining popularity due to its efficiency in recent years. Now it is extensively used for the characterization of electrochemical reactions and complex interfaces. Different ac frequencies are used for the measurement and later name 'impedance spectroscopy' was adopted. Information about structure, interface and ongoing reaction can be analyze from the system response. It has become very important technique in the field of research and applied chemistry. Besides its importance, it is a very sensitive technique too which must be used with great care and efficiency [16, 17].

The measurement of capacity of the circuit to oppose the flow of charges is called impedance. It gives reference to the frequency dependent resistance which is given by current having specific frequency.
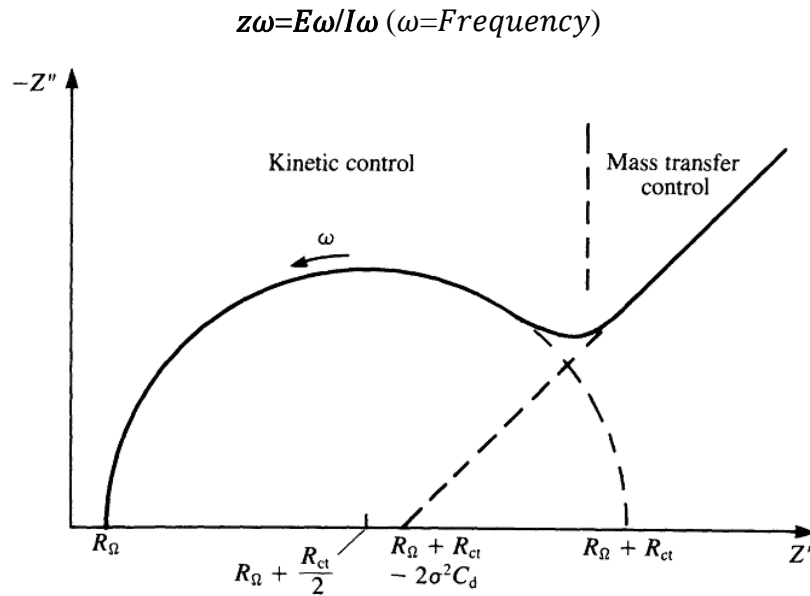
$$z\omega=E\omega/I\omega \; (\omega=Frequency)$$



Figure 0.8 Nyquist plot

EIS data can be presented as Nyquist plot or Bode plot. Usually Nyquist plot take into account when it comes to impedance studies. A typical Nyquist plot has shown in Figure.1.20. It provides measurement of capacitance, help in the identification of diffusion-limited process and information about the rate of overall electrochemical process occurring on the electrode [18].

### 3.3.3 Chronoamperometry (CA)

It is an electrochemical method in which potential of the working electrode stopped and current produce from the faradic processes at the electrode is monitored carefully with respect to time. Stability of catalyst can be measured by using this technique in electrochemical studies. Since the current is incorporated for the longer rime intervals, so this technique gives better signal to noise ratio in contrast to other ampere-metric techniques used for this purpose.
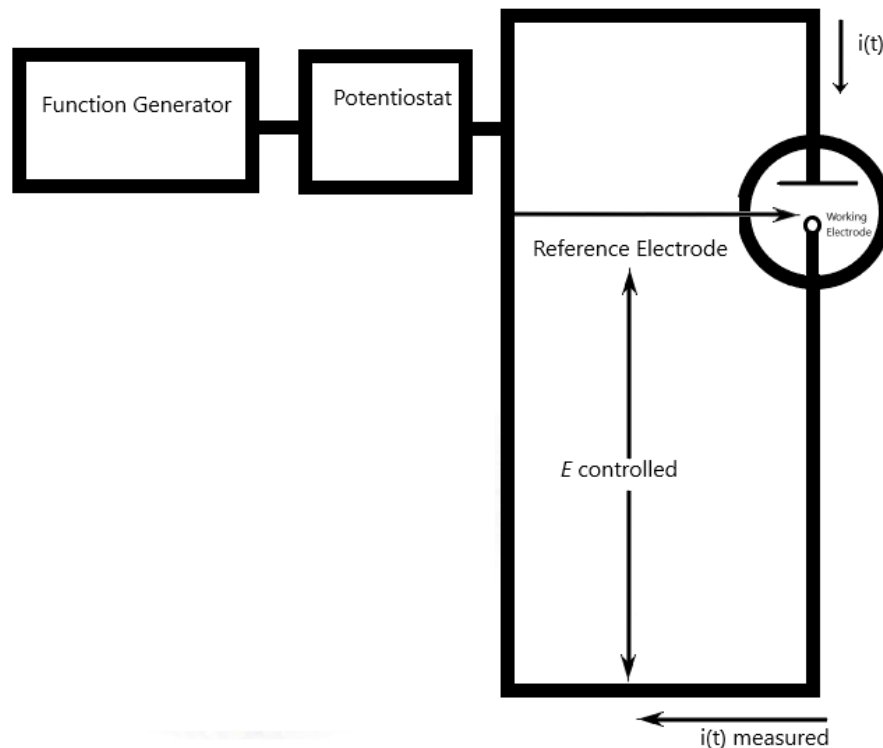
Figure 0.9 Workimg principle of CA

The three electrode system used for this technique is same as that used for CV and EIS. A prolonged time period is required for chronoamperometry to measure the consistency and analyze the sustainability of the material. Usually fixed area of electrode is used in chronoamperometry which is suitable for electrode processes of coupled chemical reactions specifically the mechanisms of organic electrochemistry. A fixed potential is applied to carry out the measurement for a specific period of given time [19].

For determination of reduction potential of analyte, cyclic volatametries run through the system. Usually fixed area of electrode is used in chronoamperometry which assist in the studies of electrode processes of coupled chemical reactions specifically in the study of reaction mechanism of organic electrochemistry.

F.G. Cottrell deduced the linear diffusion on a planer electrode by diffusion law and Laplace transformation and he obtained Cottrell equation:

$$i = \frac{nFAC\sqrt{D}}{\sqrt{t\pi}}$$

Different electrodes have different relationship among E and t in chronoamperometric graph. In such circumstances, E is the electrode potential in voltage and t in chronopotentiometry graph. This technique can produce stable current that can flow among two different electrodes.

## Summary

This chapter initially discusses different chemical synthesis methods like solvothermal and hydrothermal method. After that material characterization techniques have been studied i.e., XRD, SEM, EDS, XPS, TEM and FTIR. Main principle of these techniques has been noted down along with diagrams. After that the whole electrochemical testing process implemented was explained including ink formation, ink deposition on substrate and electrochemical performance determination using various techniques like CV, CP, and EIS with a three-electrode system.

# References

[1] B. C. Smith, *Fundamentals of Fourier transform infrared spectroscopy*. CRC press, 2011.

[2] I. Noda, "Two-dimensional infrared spectroscopy," *Journal of the American Chemical Society,* vol. 111, no. 21, pp. 8116-8118, 1989.

[3] M. Eckert, "Max von Laue and the discovery of X- ray diffraction in 1912," *Annalen der Physik,* vol. 524, no. 5, pp. A83-A85, 2012.

[4] M. von Laue, "Concerning the detection of X-ray interferences," *Nobel lecture,* vol. 13, 1915.

[5] R. Snyder, D. Bish, and J. Post, "Modern powder diffraction," *Reviews in mineralogy,* vol. 20, pp. 101-144, 1989.

[6] J. I. Goldstein, D. E. Newbury, J. R. Michael, N. W. Ritchie, J. H. J. Scott, and D. C. Joy, *Scanning electron microscopy and X-ray microanalysis*. Springer, 2017.

[7] L. Reimer, *Scanning electron microscopy: physics of image formation and microanalysis*. Springer, 2013.

[8] H. Leamy, "Charge collection scanning electron microscopy," *Journal of Applied Physics,* vol. 53, no. 6, pp. R51-R80, 1982.

[9] R. R. Mather, "13 - Surface modification of textiles by plasma treatments," in *Surface Modification of Textiles*, Q. Wei, Ed.: Woodhead Publishing, 2009, pp. 296-317.

[10] D. R. Baer and S. Thevuthasan, "Chapter 16 - Characterization of Thin Films and Coatings," in *Handbook of Deposition Technologies for Films and Coatings (Third Edition)*, P. M. Martin, Ed. Boston: William Andrew Publishing, 2010, pp. 749-864.

[11] M. H. Engelhard, T. C. Droubay, and Y. Du, "X-Ray Photoelectron Spectroscopy Applications," in *Encyclopedia of Spectroscopy and Spectrometry (Third Edition)*, J. C. Lindon, G. E. Tranter, and D. W. Koppenaal, Eds. Oxford: Academic Press, 2017, pp. 716-724.

[12] A. Parupudi, S. H. R. Mulagapati, and J. A. Subramony, "Chapter 1 - Nanoparticle technologies: Recent state of the art and emerging opportunities," in *Nanoparticle Therapeutics*, P. Kesharwani and K. K. Singh, Eds.: Academic Press, 2022, pp. 3-46.

[13] P. S. Kumar, K. G. Pavithra, and M. Naushad, "Chapter 4 - Characterization techniques for nanomaterials," in *Nanomaterials for Solar Cell Applications*, S. Thomas, E. H. M. Sakho, N. Kalarikkal, S. O. Oluwafemi, and J. Wu, Eds.: Elsevier, 2019, pp. 97-124.

[14] P. T. Kissinger and W. R. Heineman, "Cyclic voltammetry," *Journal of Chemical Education,* vol. 60, no. 9, p. 702, 1983.

[15] G. A. Mabbott, "An introduction to cyclic voltammetry," *Journal of Chemical education,* vol. 60, no. 9, p. 697, 1983.

[16] M. E. Orazem and B. Tribollet, *Electrochemical impedance spectroscopy*. John Wiley & Sons, 2017.

[17] A. Lasia, "Electrochemical impedance spectroscopy and its applications," in *Modern aspects of electrochemistry*: Springer, 2002, pp. 143-248.

[18] B.-Y. Chang and S.-M. Park, "Electrochemical impedance spectroscopy," *Annual Review of Analytical Chemistry,* vol. 3, pp. 207-229, 2010.

[19] J. L. Owens, H. A. Marsh Jr, and G. Dryhurst, "Electrochemical oxidation of uric acid and xanthine: an investigation by cyclic voltammetry, double potential step chronoamperometry and thin-layer spectroelectrochemistry," *Journal of Electroanalytical Chemistry and Interfacial Electrochemistry,* vol. 91, no. 2, pp. 231-247, 1978.

# Chapter 4:

# Experimental work

This chapter explains all the experimental work done in the laboratory and introduces different suitable synthesis techniques employed to synthesize desired materials. This chapter basically consists of two sections in which one section explains synthesis of catalyst and second part describes electrochemical assembly.

## 4.1 Synthesis of mono-metallic Co/NPC

Co/NPC was synthesized by simple solution method according to reported approach [1].

### 4.1.1 Materials

Cobalt nitrate hexahydrate ($Co(NO_3)_2.6H_2O$), 2-methyl imidazole (MIM), and methanol ($CH_3OH$). All materials are provided by sigma-Aldrich and Merck and were used without any further treatment.

### 4.1.2 Equipment

Hot plate, centrifuge machine and vacuum oven.

### 4.1.3 Method of preparation

Preparation of frameworks was confronted preponderant difficulties. Fortunately, solution mixing technique was established to be favorable explication to these problems[2].

1. The cobalt nitrate hexahydrate (4m.mol) and 2-methylimidazole (16m.mol) were dissolved in 50mL of methanol separately.
2. Then the 2-MIM solution was mixed in the cobalt nitrate solution by continuous stirring on magnetic stirrer until the two solution were completely dissolved.
3. Then the mixture was placed for 24hrs for aging.
4. The purple precipitates were obtained, which were collected, washed, and dried at 60°C for 7 hrs.
5. The resultant material was pyrolyzed in a tube furnace with the stay at 350°C for 1hr and then the temperature was elevated to 700°C for 3.5hr under $H_2/Ar$ atm (10/90).

## 4.2 Synthesis of bi-metallic MnCo/NPC

MnCo/NPC were also prepared by simple solution mixing technique.

### 4.2.1 Materials

Manganese nitrate hydrate ($Mn(NO_3)_2.H_2O$), Cobalt Nitrate hexahydrate ($Co(NO_3)_2.6H_2O$), 2-methylimidazole ($C_4H_6N_2$), and ethanol ($C_2H_5OH$)were purchased from Sigma Aldrich. DI water was used throughout the experiment.

### 4.2.2 Equipment

Hot plate, centrifuge machine and vacuum oven.

### 4.2.3 Method of preparation

1. The manganese nitrate hydrate (4m.mol) and as-synthesized ZIF-67 were taken in 40mL ethanol and then stirred for 30 min at rpm of 350 on magnetic stirrer
2. Then the material was collected by centrifugation, washed several times with ethanol and dried in vacuum oven at a temperature of 70˚C for 6hrs [3].
3. The resultant light purple material was pyrolyzed in a tube furnace with the stay of 1hr at 350˚C and then the temperature was elevated to 700˚C for 3.5hr under $H_2$/Ar atm (10/90).

## 4.3 Synthesis of ternary-metal NiMnCo/NPC

NiMnCo/NPC were prepared by impregnation method.

### 4.3.1 Materials

Nickel Nitrate hexahydrate ($Ni(NO_3)_2.6H_2O$), and ethanol ($C_2H_5OH$).

### 4.3.2 Equipment

Vacuum oven

### 4.3.3 Method of preparation

1. The nickel nitrate hexahydrate (32m.mol) was impregnated on the as-synthesized MnCo/NPC.
2. After impregnation, the dirty green material was then heated at 70˚C for 9hrs and then calcined at 350˚C for 2hr in muffle furnace.
3. The resultant product obtained was Ni doped MnCo/NPC based nitrogen nano-porous carbon.
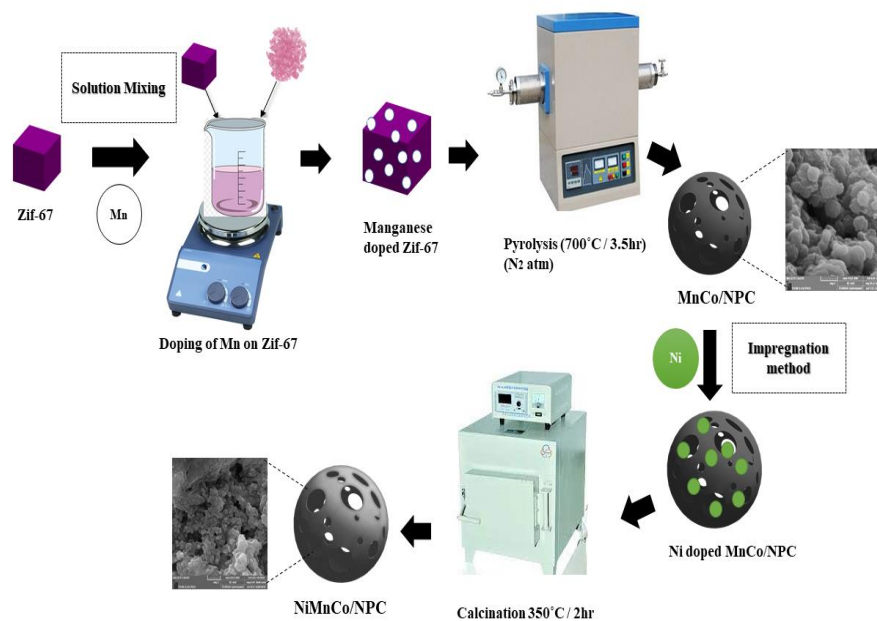
Figure 0.1 Schematic diagram of synthesis of NiMnCo/NPC

## 4.4 Electrochemical assembly

Electrochemical testing was conducted in 1M KOH and 3M $CH_3OH$ through traditional 3-electrode system by using techniques like Chronoamperometry (CA), Cyclic Voltammetry (CV), and Electrochemical Impedance Spectroscopy (EIS). The system was assisted by the Reference Gamry Instrument 3000/3000AE facilitated with software version 7.06. This system consist of a counter electrode (platinum wire), reference electrode (silver/silver chloride), and working electrode (ink of the as-synthesized material) was deposited over the glassy carbon(GC) surface.



Figure 0.2 Illustrated diagram of electrochemical workstation

### 4.4.1 Preparation of ink slurry

Catalytic ink was made by combining 2mg of catalyst, 80µL ethanol , and a Nafion of 5 wt% solution (20µL). Before each electrochemical experiment, on a glassy carbon electrode a drop of 1.5µL of ink was placed. The above mentioned electrode was allowed to dry at ambient temperature. At a voltage window spanning from 0.0 to 0.6 V and several scan rates, complete testing of generated samples was carried out.



Figure 0.3 Coating of slurry on GCE

**Summary**

This chapter includes the total experimental procedure that was involved in the research process. The synthesis process of Co/NPC, MnCo/NPC, and NiMnCo/NPC used were thoroughly demonstrated in the chapter. Finally, the electrochemical testing techniques which were used on electrochemical workstation and the testing parameters are discussed.

# References

[1]      A. Abbasi, M. Soleimani, M. Najafi, and S. Geranmayeh, "New interpenetrated mixed (Co/Ni) metal–organic framework for dye removal under mild conditions," *Inorganica Chimica Acta,* vol. 439, pp. 18-23, 2016.

[2]      C. Dey, T. Kundu, B. P. Biswal, A. Mallick, and R. Banerjee, "Crystalline metal-organic frameworks (MOFs): synthesis, structure and function," *Acta Crystallographica Section B: Structural Science, Crystal Engineering and Materials,* vol. 70, no. 1, pp. 3-10, 2014.

[3]      X. Chen *et al.*, "ZIF-67-derived Mn doped Co9S8 supported on N-Enriched porous carbon polyhedron as an efficient electrocatalyst for oxygen evolution reaction," *International Journal of Hydrogen Energy,* vol. 46, no. 78, pp. 38724-38732, 2021/11/11/ 2021.

# Chapter 5:

# Results and Discussion

## 5.1 Characterization

Surface morphologies were studied by technique Scanning-electron microscopy (SEM) (VEGA3 TESCON) at a voltage of 20 kV and various resolutions. At three distinct locations for investigation of the elemental analysis of as-synthesized compounds, Energy dispersive spectroscopy i.e., EDS technique with SEM was also employed. The structure analysis of the composite was observed using an X-ray powder diffractometer (XRD STOE Germany). The diffraction angle ($2\theta$) with a step size of 4° was changed at a range of 5–80° using an XRD machine attached to a computer interface with Cu K at =1.5418. The co-ordination of metal ligands was observed by using Fourier-transform infra-red spectroscopy (Perkin spectrum 100 FT-IR spectrophotometer) in the wave number range of 500–4000 cm$^1$.

### 5.1.1 X-Ray diffraction (XRD)

The microstructure determines the electrocatalytic characteristic of Co/NPC, MnCo/NPC and NiMnCo/NPC composites. XRD is used for the structure analysis of the as-synthesized NPC/ Co/NPC, MnCo/NPC, and NiMnCo/NPC composites, as illustrated in Figure 2. The diffraction peak to a typical (002) interlayer peak at about $2\theta = 25°$, found in Co/NPC confirm of carbon sheets (graphite-type) and diffraction peaks generated from crystalline Co at $2\theta = 45°$, were also observed [1].
The XRD patterns of MnCo/NPC and NiMnCo/NPC reveal broad peaks at $2\theta=24°$, correspondent to the typical peaks of graphitic carbon (002)[2] and the characteristic peak of the MnOx phase ($2\theta = 43°$, and 63°) correlates to the (111), and (002) planes, respectively [3]. XRD pattern of NiO reveal primary diffraction peaks that were indexed at $2\theta= 62$, 75.3 crystal planes (220 and 311) with a cubic structure, which is consistent with literature[4]. The peaks obtained in NiMnCo/NPC composite are more pronounced than MnCo/NPC because of their crystalline form, overlapping of major peaks of metals at this size might be the reason. The presence of no additional impurity-related peak in

the Co/NPC, MnCo/NPC, and NiMnCo/NPC XRD spectra proved their exceptional purity and crystallinity.

Inter-layer distance (d-spacing) for the angle $\theta=25°$ (002 peak) calculated was 0.34 nm, this is consistent with the literature[5, 6]. By the addition of manganese and nickel in bi-metallic nano porous carbon and tri-metallic nano porous carbon the value of d-spacing is increased to 0.416 nm and 0.419 nm. EDX spectrometry was further used to verify their compositions.
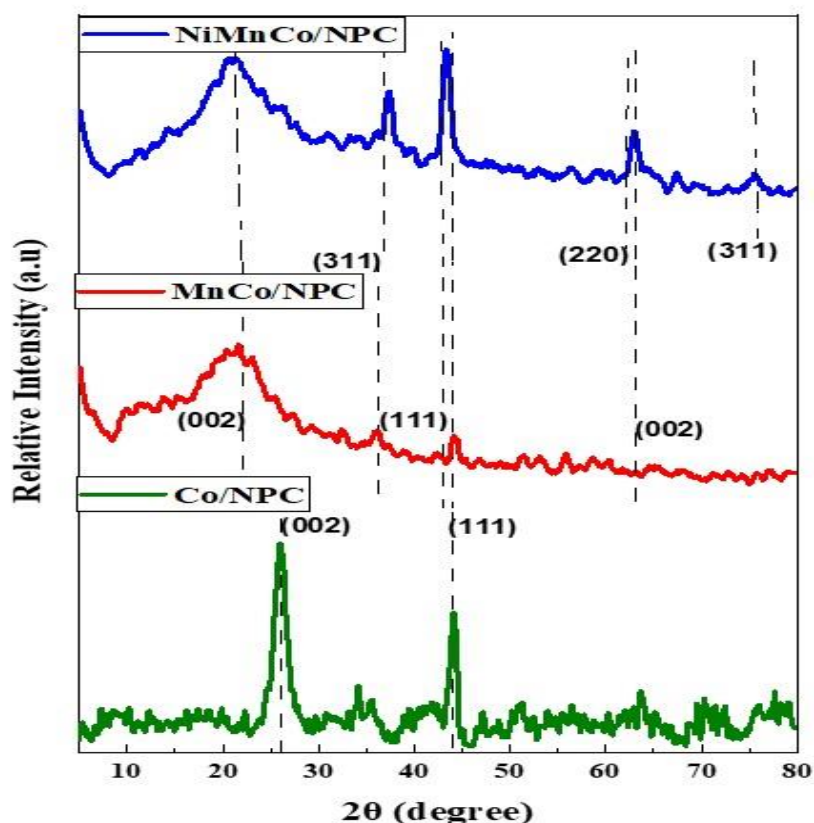
Figure 0.1 XRD of Co/NPC, MnCo/NPC, and NiMnCo/NPC

### 5.1.2 Scanning electron microscopy (SEM)

SEM was used to examine the morphology of MnCo/NPC and NiMnCo/NPC, as shown in Figure 3. The SEM pictures revealed a spherical shape, but not the characteristic Zif-67 rhombic form. It is possible that manganese and nickel have been doped. The aforesaid substance has also been pyrolyzed and calcined.
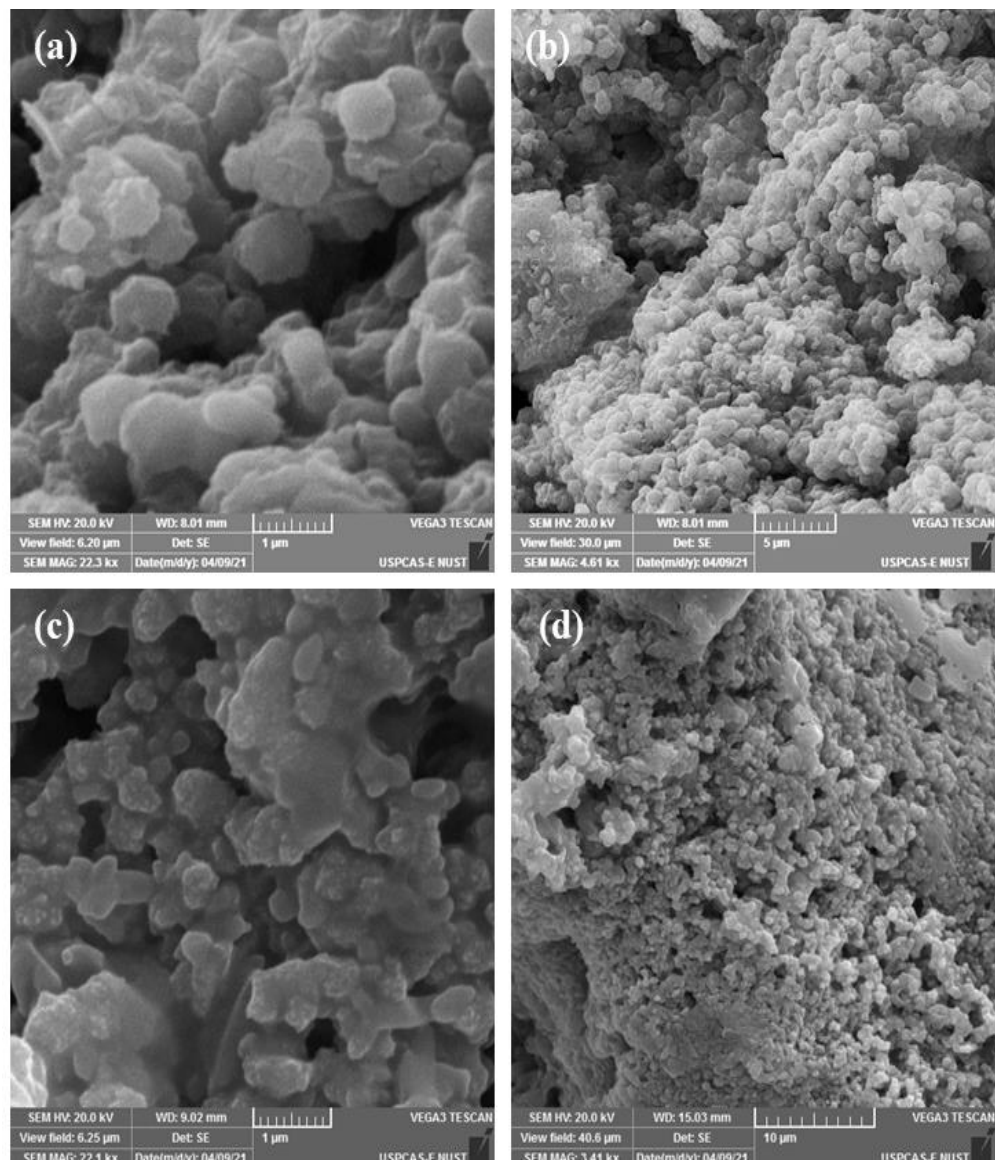
Figure 0.2  SEM results of MnCo/NPC (a,b) and NiMnCo/NPC (c,d)

### 5.1.3 Energy dispersive X-ray Spectroscopy (EDS)

The EDX analysis of MnCo/NPC and NiMnCo/NPC indicates the presence of oxygen, carbon, and nitrogen, as well as nickel, manganese, and cobalt, as shown in Table 1. The EDS result revealed no contaminants.
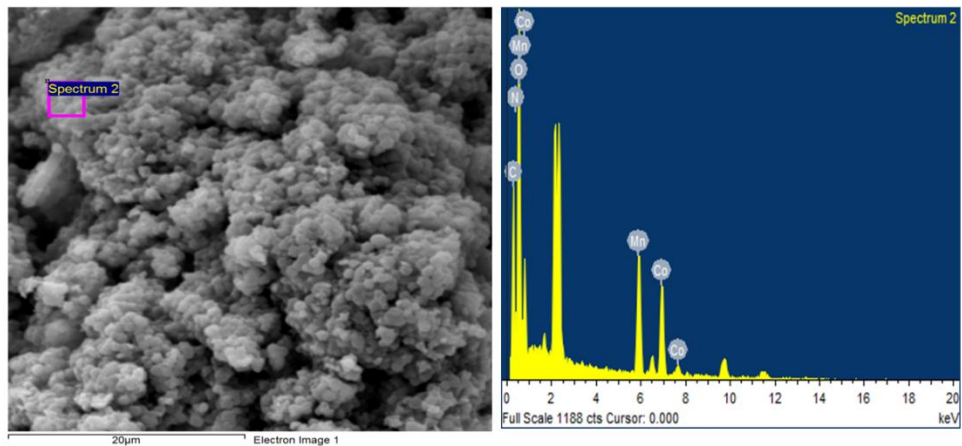
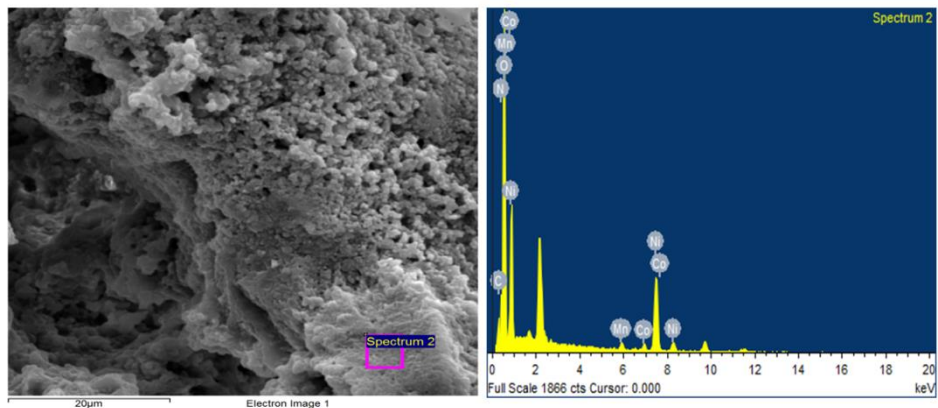Figure 0.3  EDS graph showing various components in MnCo/NPC



Figure 0.4  EDS graph showing various components in NiMnCo/NPC

Table 0.1  Comparison of EDS result of  MnCo/NPC, NiMnCo/NPC

| Sample | MnCo/NPC | NiMnCo/NPC |
|---|---|---|
| C wt% | 8.96 | 18.97 |
| O wt% | 42.36 | 41.36 |
| N wt% | 4.55 | 3.85 |
| Co wt% | 28.97 | 5.04 |
| Mn wt% | 15.16 | 5.18 |
| Ni wt% | - | 25.60 |

**5.1.4 Fourier Transform Infrared spectroscopy (FTIR)**

FTIR investigation corroborated the vibrational atom modes of Co/NPC, MnCo/NPC, and NiMnCo/NPC nanocomposites, as illustrated in Figure 5. The –OH vibration mode of water is suggested by the vibration at 3400 cm[1][7]. The C-H bond of the aromatic ring is noticed at a peak of 3040-3060 cm[1], while the C-N band of the amide bond is observed at a peak of 1240 to 1340 cm[1]. The bending vibrations of O–H coupled with the Mn atoms are allocated to the absorption bands about 1627 and 1036 cm[1][8]. Inter-atomic vibrations produce absorption bands below 800 cm[1] in metal oxides such as Ni-O, Co-O, and Mn-O. The features of the Co-O stretching vibrations in $Co_3O_4$ are shown by the unique band at 576 cm[1][9].
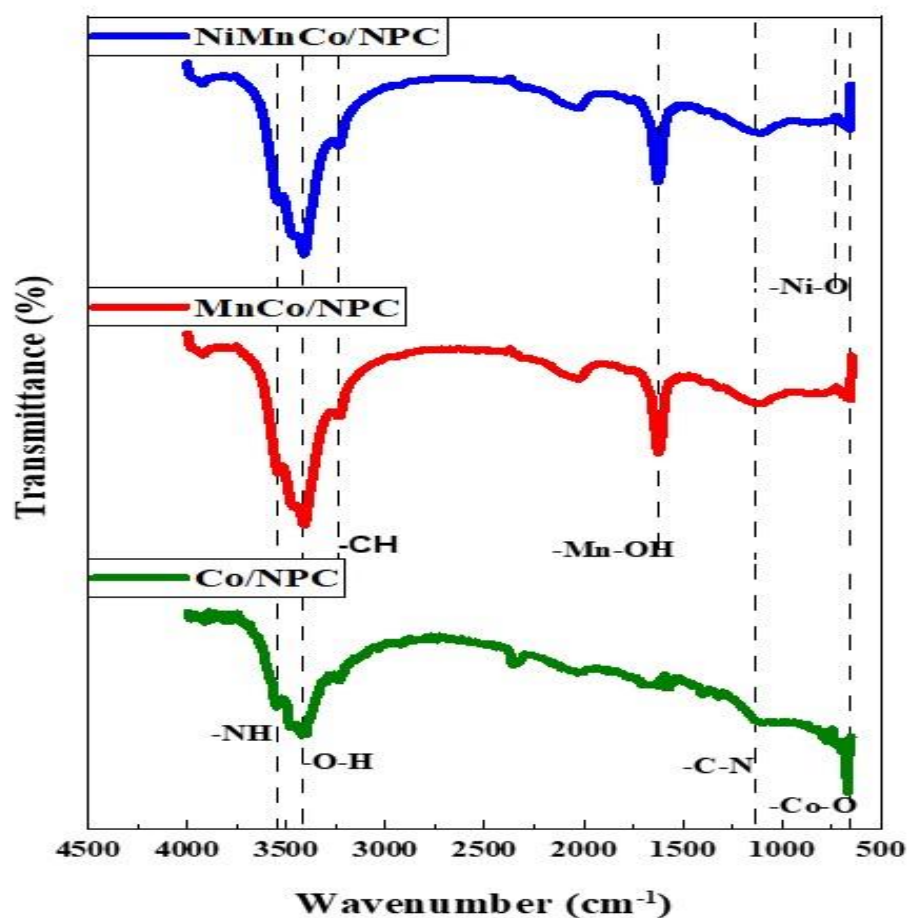


Figure 0.5  FTIR results of Co/NPC, MnCo/NPC, and NiMnCo/NPC

### 5.1.5 Transmission Electron Microscope (TEM)

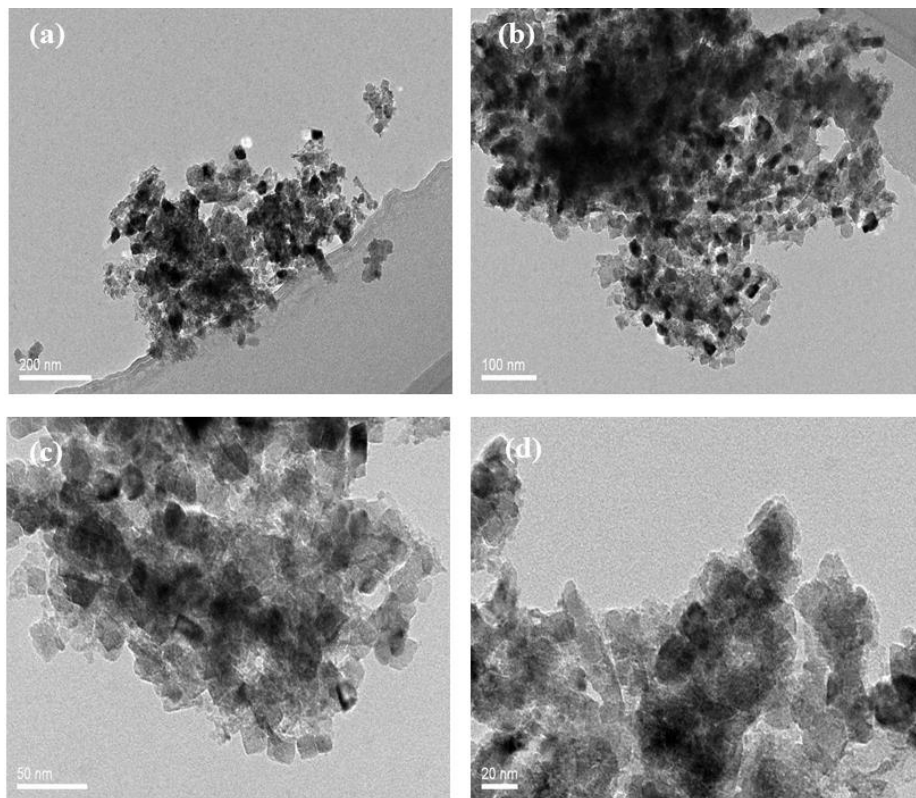TEM examination confirmed the existence of tiny spherical nanoparticles having nano-porous structure.



Figure 0.6  TEM results of NiMnCo/NPC (a) 200 nm (b) 100 nm (c) 50 nm (d) 20 nm

### 5.1.6 X-ray photoelectron spectroscopy (XPS)

The metal oxidation states and chemical compositions of the calcinated products were confirmed by XPS analysis. Figure 6a shows the survey XPS spectrum, which matches the XRD results for Co, Mn, Ni, N, C, and O elements. $Ni(OH)_2$ and the substrate can both be used to produce Ni. The Mn 2p spectra shows two distinct peaks for $2p_{1/2}$ (653.1) and $2p_{3/2}$ (641.5 eV) (Fig. 6d), with $Mn^{2+}$ peaks (652.3 and 653.3 eV) and $Mn^{3+}$ (640.9 and 642.4 eV)[10]. Because of the oxidation of $Mn_3O_4$ following exposure of air, the $2p_{1/2}$ (654.5 ) and $2p_{3/2}$ peaks (646.4 eV) were ascribed to $Mn^{4+}$. Two primary peaks for Co $2p_{1/2}$ (795.8 eV) and Co $2p_{3/2}$ (779.8 eV) were found in the Co 2p spectra (Figure 6e), where these peaks belong to $Co^{3+}$.[11].

The Ni 2p high-resolution spectrum is shown in Figure 6c. The Ni $2p_{3/2}$ and Ni $2p_{1/2}$ peaks, respectively, are located at 852.4 and 867.5 eV. Deconvolution of the Ni 2p spectra provides two $Ni^0$ fitting peaks with binding energies of 852.2 and 867.2 eV, and two $Ni^{2+}$ fitting peaks at 854.0 and 869.2 eV[12]. The three primary peaks in the O 1s spectrum (Figure 6b) correspond to M–O, M–OH, and surface-adsorbed water molecules, respectively, and are located at 529.3, 530.4, and 530.9 eV[10].

To analyze the N chemical state, fine-scanned N 1s spectra were fitted (Figure 6g). By deconvoluting the N peak, three different forms of nitrogen may be obtained: pyridinic N, pyrrolic N, and graphitic N at 398.4 eV, 400.1 eV, and 401.1 eV, respectively[13]. The XPS of C 1s may be deconvoluted into three peaks (Figure 6f), each centered at 284.6, 285.6, and 288.8 eV and assigned to C-C/C=C, C-N, and C=O species, respectively[14].
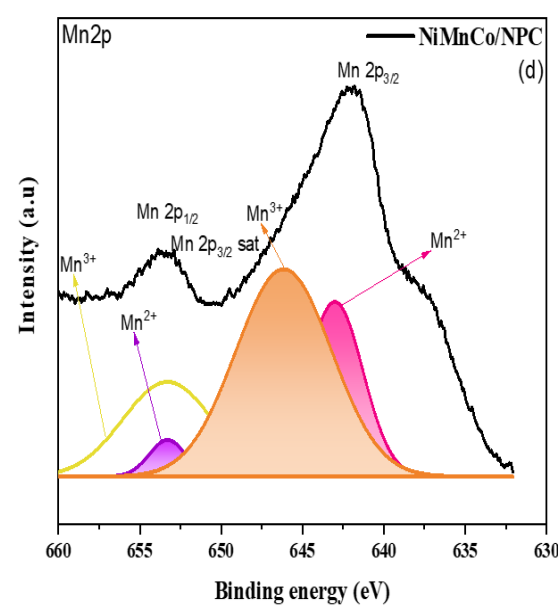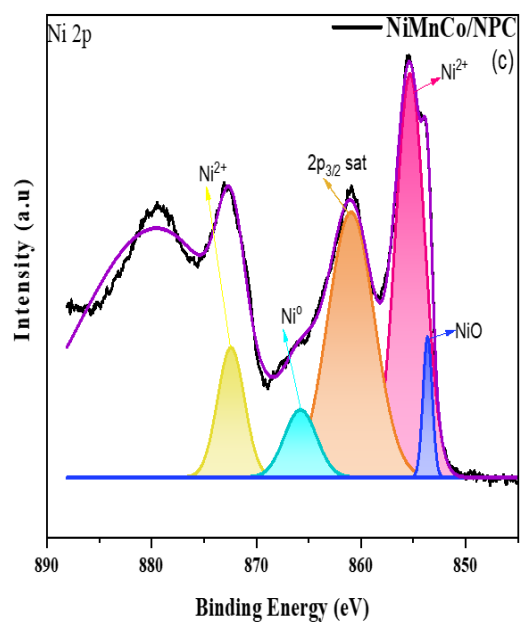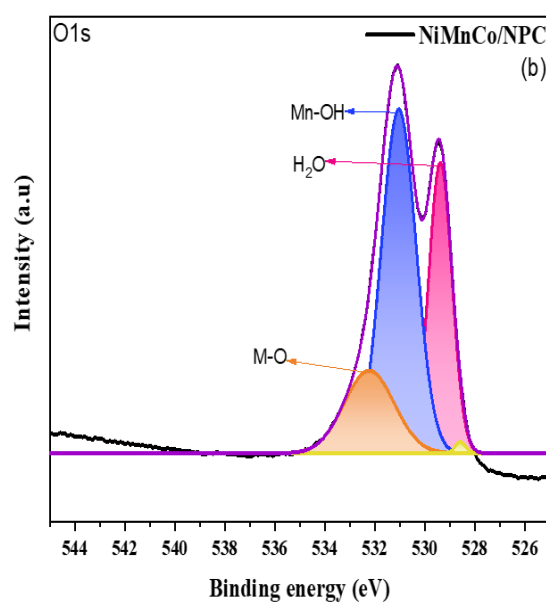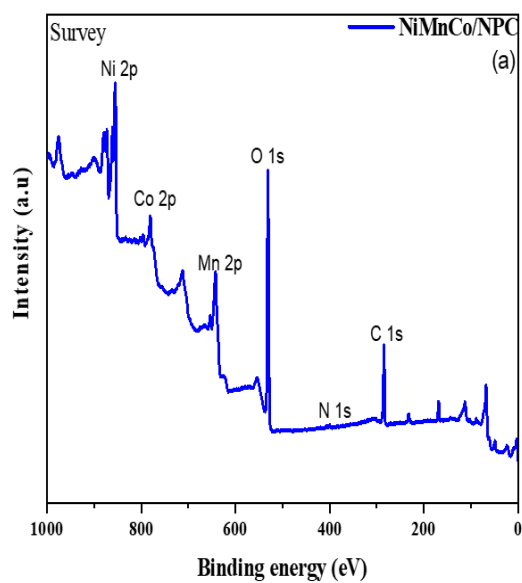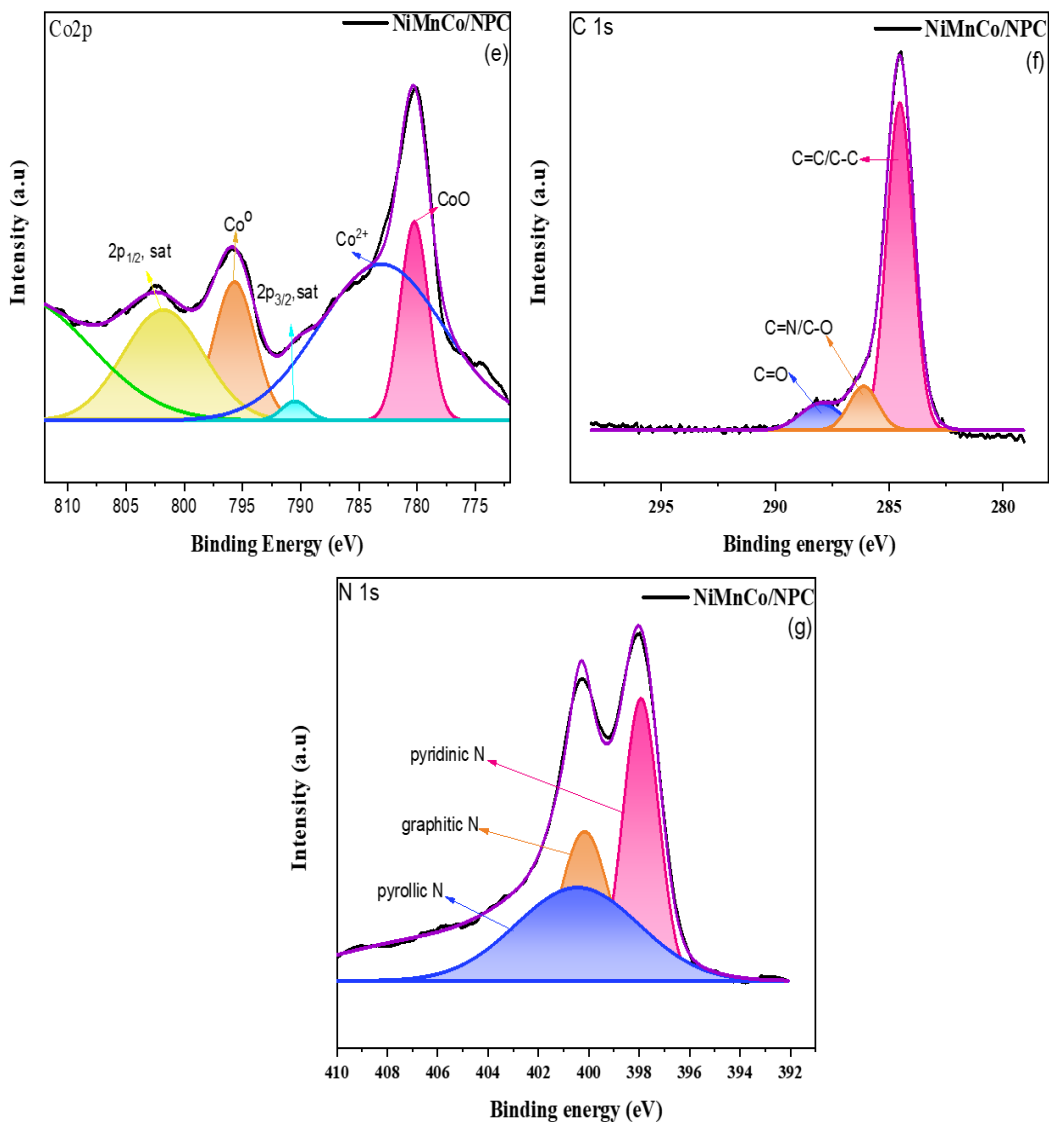
Figure 0.7  XPS of NiMnCo/NPC

## 5.2 Electrochemical studies

A three electrode system was used for all electrochemical studies by using 1M NaOH as supporting electrolyte and 3M methanol as fuel. Glassy carbon electrode (GCE) was used as working electrode and Ag/AgCl was used as reference and Pt wire was used as counter electrode. Nafion served as efficient binding agent here. Scan results were taken from modified GCE. To explore the influence of scan rate, cyclic voltammetry was used

to test electrochemical performance in an alkaline electrolyte at a scan rate between 0.0 V and 1.0 V.

## 5.2.1 Cyclic voltammetry

GAMRY G750 in potentiostatic mode was utilized for conducting electrochemical studies.

### 5.2.1.1 Effect of different Scan rate

The peak current densities showed linear relationship of composites such as single metal Co/NPC, bimetallic MnCo/NPC, and ternary NiMnCo/NPC with scan rates ranging from 50 to 200mV/s as demonstrated in Figure 7. With the increase in scan rate, gradual increase in peak current density is observed. Non-electroactive species are neither oxidized or reduced into the product, which results in a high current density at a faster scan rate. Because of the generation of electroactive products, a high current density is achieved[15]. It can be deduced from the data that raising the scan rate, i.e., 50mV/s–200 mV/s for all composites, will result in an increase in current density. The catalytic material's reaction response is linked to the increased scope of reaction. Furthermore, increasing the scan rate likely increased electron mobility[16].
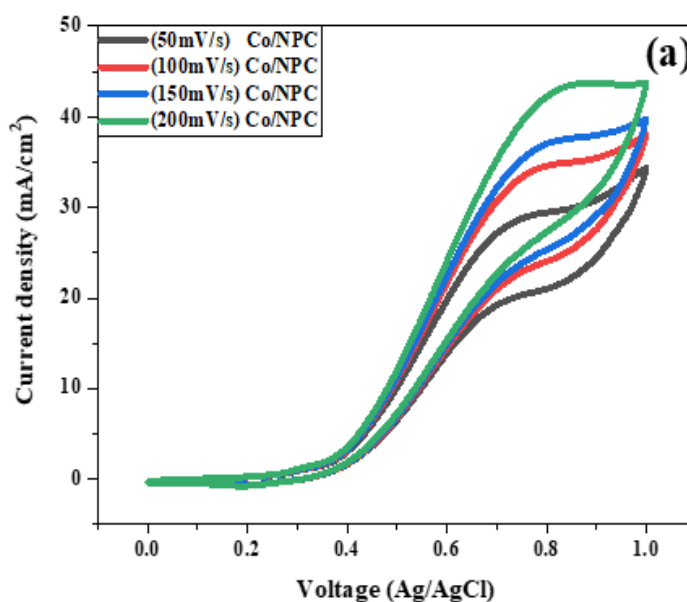
Figure 0.8 CV results of (a) Co/NPC, (b) MnCo/NPC, (c) NiMnCo/NPC at various scan rates

**5.2.1.2 Comparison of CV curve of mono-metallic, bi-metallic, and ternary metal**

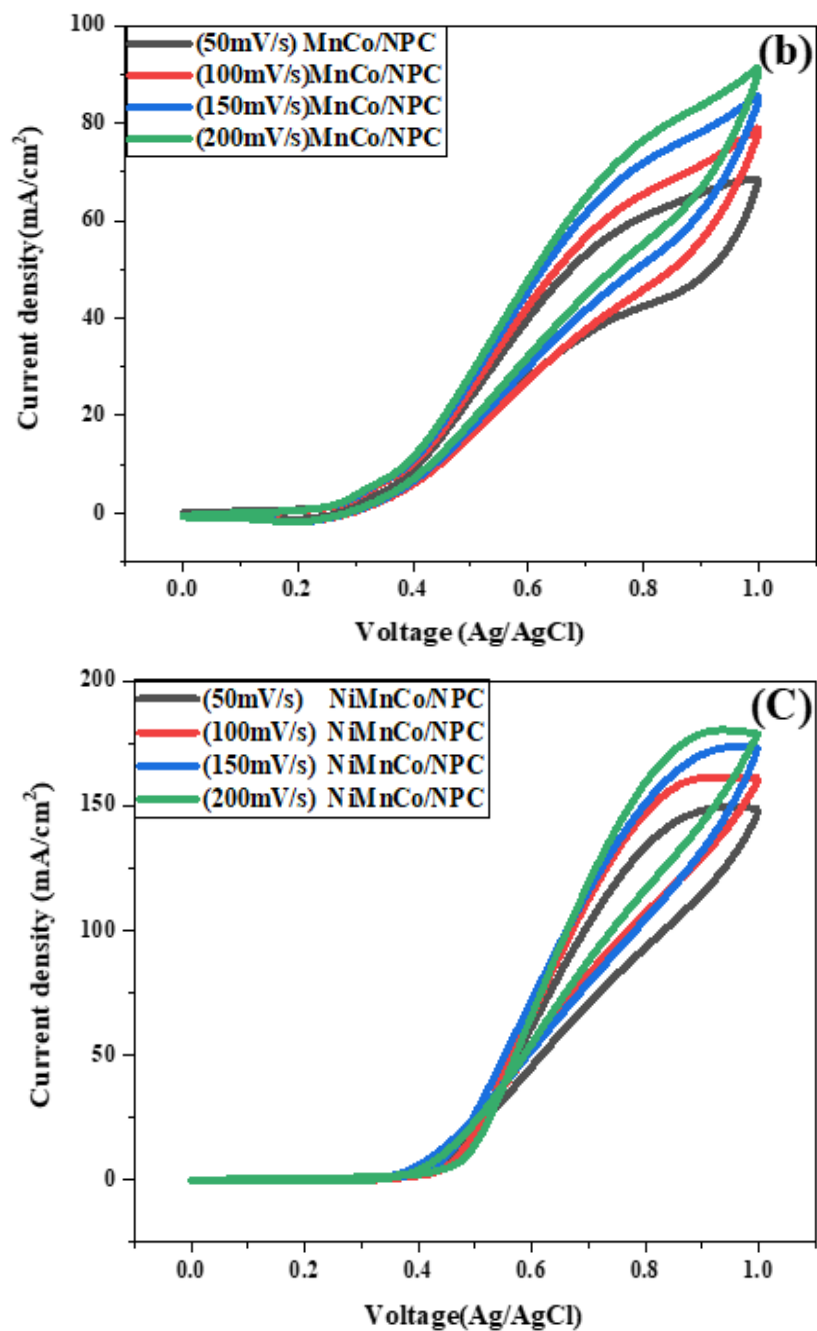Comparative scans of all the catalysts were taken by running Potentio-static scan with three electrode system in 1M NaOH and 3M $CH_3OH$ to observe the gradual change in

response of catalysts by the addition manganese and nickel. Results clearly demonstrate the participation of metals in enhancing catalyst conductivity and efficiency by increasing the surface area. High concentration of nickel metal enhanced the electro catalytic activity for MOR.

The current density of Co/NPC at 50mV/s was 28.72 mA/cm$^2$, but when Mn was added, the peak current density increased to 63.35mA/cm$^2$ of MnCo/NPC. NiMnCo/NPC, a ternary Ni doped MnCo/NPC, has the greatest peak current density of 147.85mA/cm$^2$ at 50mV/s as illustrated in Figure 8. Furthermore, the CV curves for single metal, bimetallic, and ternary Zif composites have varied shapes and peak positions due to the addition of different metals, and by adding these metals, the capacitive surface area rises, which improves the electrochemical capabilities of the catalyst. In comparison to bimetallic MnCo/NPC and single metal Co/NPC, ternary NiMnCo/NPC showed significant increases in peak current density and peak potential, indicating that the ternary electrocatalyst is more efficient.
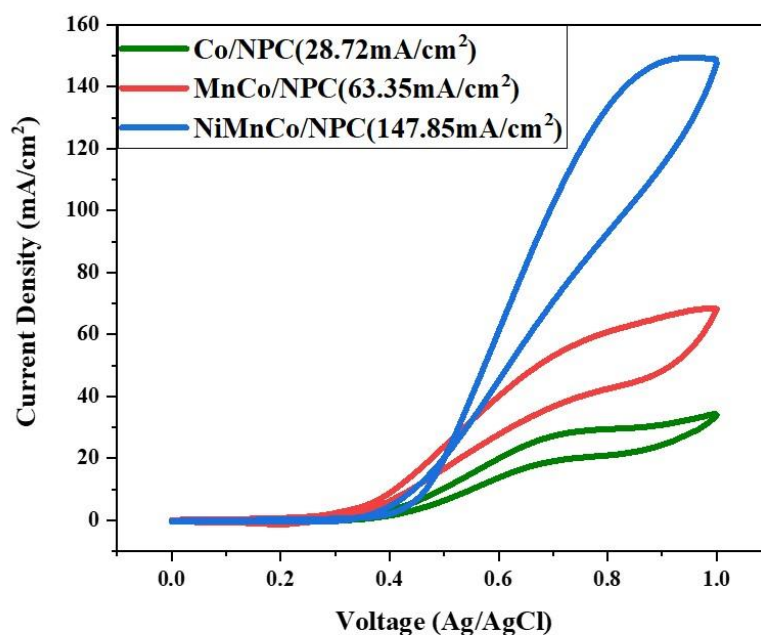


Figure 0.9  Comparison of CV of Co/NPC, MnCo/NPC and NiMnCo/NPC at 50 scan rate

We have not gone above 200mV/s scan rate because the reaction rates will fast extensively and little time that it does not allow the reaction to take place due to slow kinetics of the system. It requires sufficient amount of time for electroactive species to diffuse first from bulk solution to the surface of electrode and then oxidize into products (carbon dioxide, electrons and protons) on the surface of electrode (anode). So, no peak of methanol oxidation was observed above scan rate 200mV/s.

Gradual increase in current density with the increase in scan rate indicates the obeying of Randles-Sevick principle. Depleted diffusion layers also results around the electrode which helps to enhance the electrocatalytic activity by abetting conduction of proton across electrolyte. Concentration gradient is increased due to the high diffusion rates of electroactive species from the bulk solution of methanol to the surface of electrode where they get oxidized or reduced to give of carbon dioxide gas, electrons that travel through external circuit to reach to the cathode and protons that diffuse through electrolyte to the cathode.

### 5.2.2 Electrochemical Impedance Spectroscopy

EIS is an excellent method to investigate the performance of catalytic material. Potentiostatic mode was used to calculate EIS impedance spectroscopy in the same three electrode system in 1M NaOH and 3M methanol with bare and modified glassy carbon electrode (GCE). Resistance present between reference electrode and working electrode must by analyzed while doing calculation of circuit electrochemical impedance although solution resistance is the dominating factor. EIS calculations are usually represented by Nyquist plot or Bode plot. In Nyquist plot Y-axis being the imaginary one while the X-axis represent real parameters because the formula for charge transfer resistance ($R_{ct}$) contains one coordinate the has one imaginary number and the other real number.

The nyquist plots for Co/NPC, MnCo/NPC, and NiMnCo/NPC are shown in Figure 11. Furthermore, the addition of nickel metal causes structural modifications that result in enhanced reaction kinetics, increased electrical conductivity, Low activation energy, least resistance to electron and ion transport, and maximal approach of reactants to active sites.
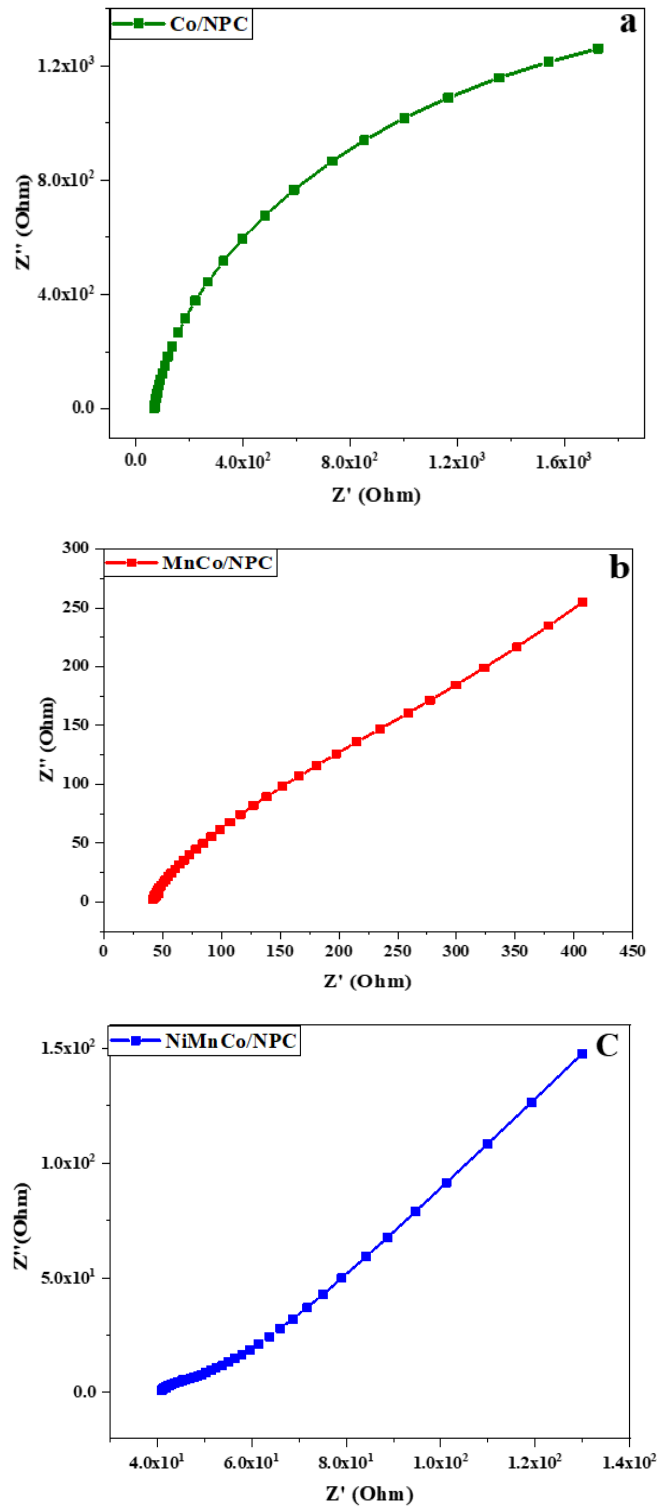
Figure 0.10  Nyquist plot of (a) Co/NPC, (b)  MnCo/NPC, and (c) NiMnCo/NPC

A linear relationship among square root of scan rate and peak current densities of prepared catalysts is shown in Figure 4.16. This plot indicates the diffusion controlled process of the system which is predominant over increased value of scan rates. Furthermore, diffusion coefficient (D) and transfer coefficient (α) can also be measured by measuring the linearity and rate constant of the charge transfer electrode and surface deposited layer.

Diffusion coefficient (D) can be calculated through Randles Sevcik equation [17]:

$$ip = (2.99 \times 105)n(\alpha n_a) \frac{1}{2} ACD \frac{1}{2} v \frac{1}{2}$$

$I_p$ = Peak current density

n = No of electrons transferred

A= Area of electrode

C= Concentration

D= Diffusion coefficient

V= Scan rate

$\acute{\alpha}$= Transfer coefficient

$n_a$=electrons in RDS



Figure 0.11 Comparison of straight line graph of Co/NPC, MnCo/NPC, and NiMnCo/NPC

65

For all the prepared catalysts the diffusion coefficient value calculated are given in Table 5.2.

Table 0.2 Diffusion Coefficent and $R^2$ value of prepared samples

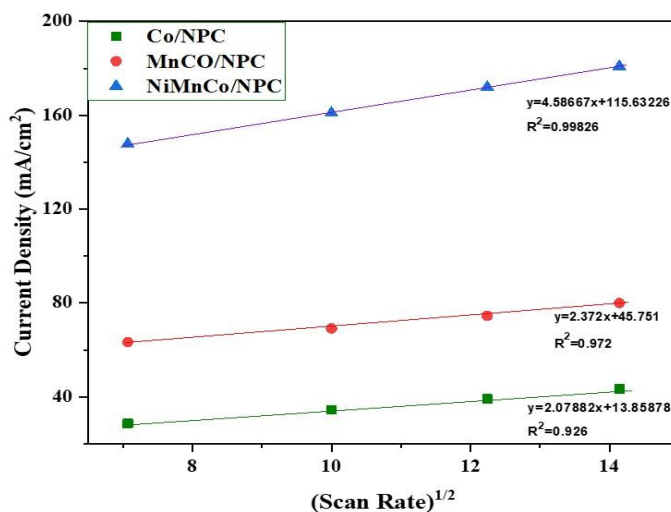| Samples | Diffusion Co-efficient ($cm^2s^{-1}$) | $R^2$ |
|---|---|---|
| Co/NPC | $2.7 \times 10^{-8}$ | 0.926 |
| MnCo/NPC | $1.33 \times 10^{-7}$ | 0.972 |
| NiMnCo/NPC | $1.50 \times 10^{-6}$ | 0.998 |

### 5.2.3 Chronoamperometry

The stability of the synthesized samples were inquired by using same electrochemical setup of three electrode system in which Glassy carbon electrode (GCE) as working electrode, Pt wire as counter electrode and Ag/AgCl act as reference electrode in 1M KOH and 3M methanol solution by chronoamperometry at 0.8V. Figure 4.17 illustrate the chronoamperometric curves of all prepared samples of electro catalysts. All these curves show comparison among Co/NPC, MnCo/NPC, and NiMnCo/NPC show stability over period of time 3600s.

It can be seen that the current value decreases to a certain value immediately after the reaction begins, which is due to the creation of an intermediate specie such as CO. After then, the current gradually decreases with time, reaching a quasi-stationary condition about 3600 seconds[18]. This might be due to methanol covering on the catalytic sites at the start of the reaction, but as the reaction progresses, an equilibrium layer of methanol forms on the surface of the catalytic sites, slowing down the entire process and affecting the stability of all the electrocatalysts[19]. In the defined time period of 3600 s, the ternary metal NiMnCo/NPC displays higher percentage stability (55.83%) among all the produced composites due to its high current density. Following that, 35.50% for bimetallic MnCo/NPC and 12.19% for monometallic Co/NPC.
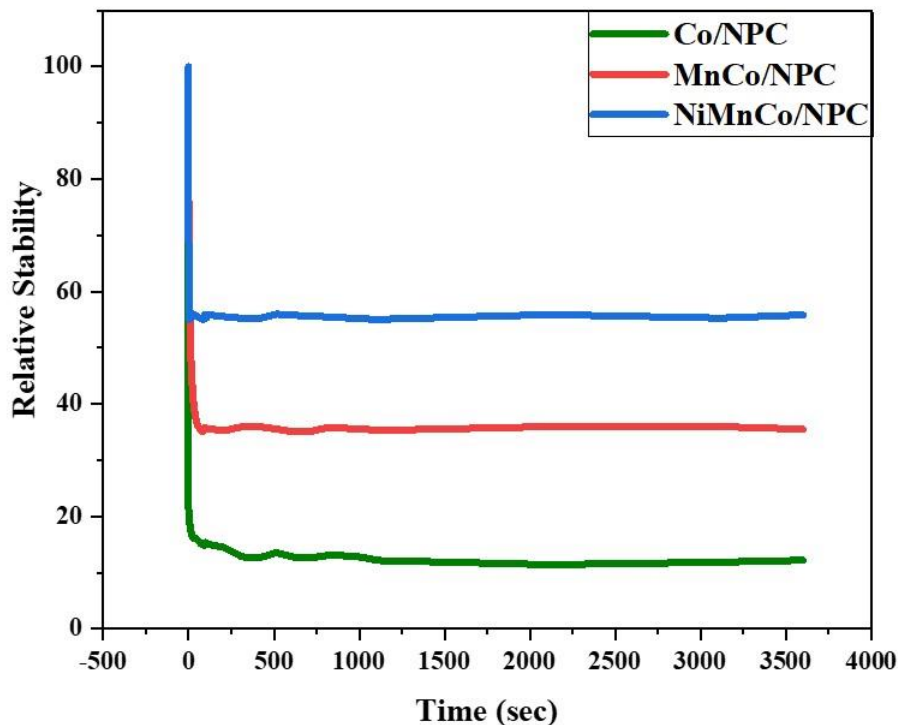
Figure 0.12 Comparison of relative stability of Co/NPC, MnCo/NPC and NiMnCo/NPC

## 5.3 Tafel studies

It is a polarization technique for the potentiostatic measurements, cyclic polarization and linear polarization resistance. It is widely used to measure the corrosion rates and faster experimental technique in comparison to the classical weight-loss estimation [20]. The NiMnCo/NPC composite has a smaller overpotential curve in this investigation. Its better electrocatalytic activity is shown in the improved overpotential at lower values, requiring less activation energy, this shows that adding metals like Ni and Mn to the catalyst may not only enhance its surface area, but also make it simpler for reactants to reach the electrode, allowing it to capture more ions and demonstrate increased activity for methanol oxidation.

In addition, for the research reaction kinetics of the catalytic process, Tafel slopes at 0.55 V of potential were determined and presented in Table 3. NiMnCo/NPC, Mn/Co/NPC, Co/NPC, have the tafel slopes of 117mV/dec, 143mV/dec and 157mV/dec

67

respectively. The slopes at lower potential might signify the first C–H bond breakage and electron transfer in methanol, which is the rate-determining step.
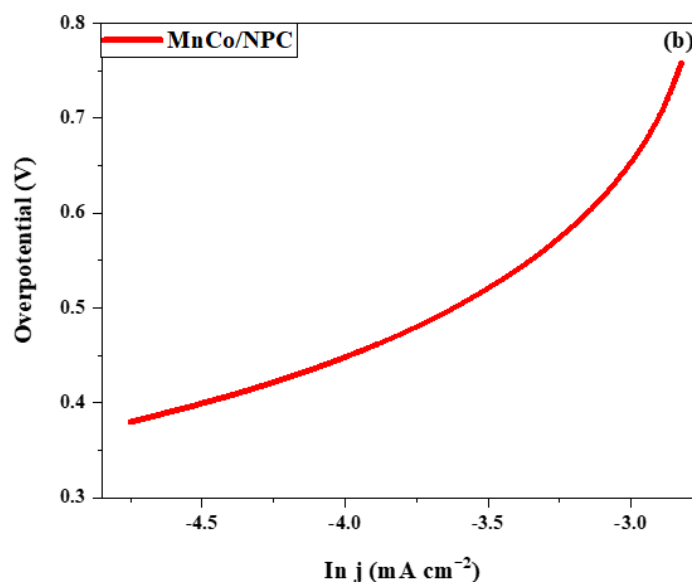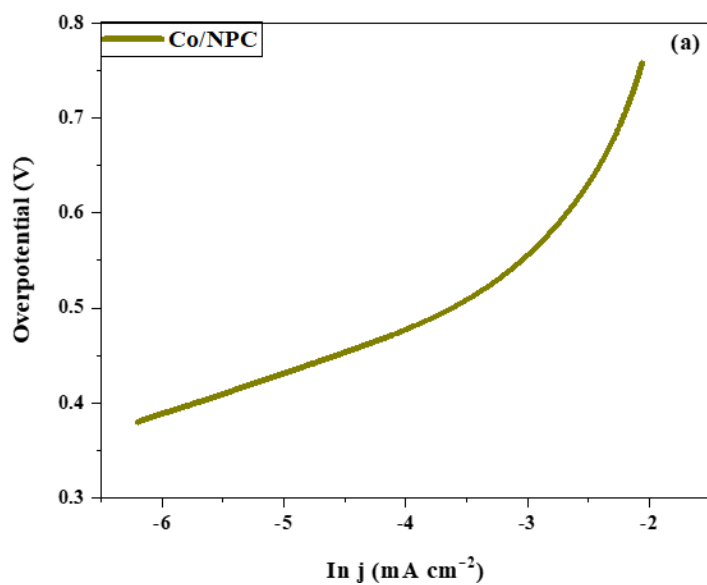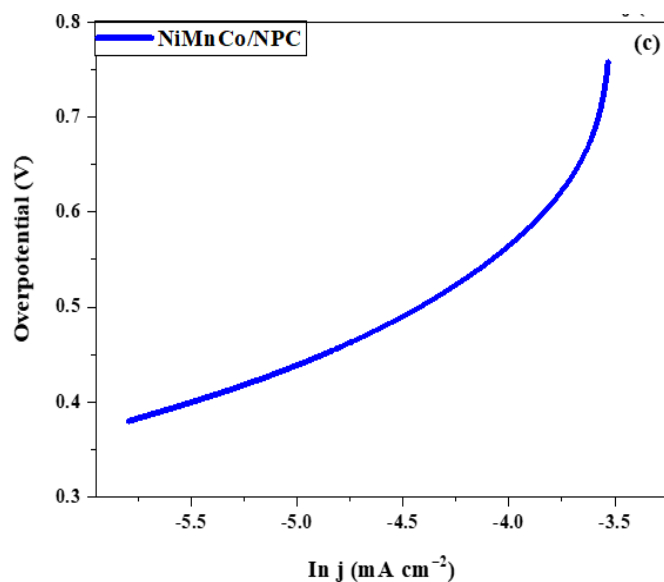
Figure 0.13 Tafel slopes of (a) Co/NPC, (b) MnCo/NPC, and (c) NiMnCo/NPC

Table 0.3  Tafel slope value of prepared samples

| Catalyst | Tafel Slope at 0.55 V (mV/dec) |
|---|---|
| Co/NPC | 157 |
| MnCo/NPC | 143 |
| NiMnCo/NPC | 117 |

## 5.4 Comparison with Literature

I have done comparison of the current densities of all prepared samples with reported catalysts for methanol oxidation reaction which showed significant results of the synthesized catalysts. $ZnO_{(60\%)}/CeO_{2(40\%)}$dots@CNFs showed current density while same catalyst with different ratio $ZnO_{(40\%)}/CeO_{2(60\%)}$dots@CNFs showed 16.3 mA/cm$^2$ while incorporation of metals like Mn and Ni rise current density as MnCo/NPC showed rise in current density upto 63.35 mA/cm$^2$ and Ni MnCo/NPC showed current density 147.85 mA/cm$^2$ . While in comparison my pure synthesized Co/NPC showed current density upto 28.72 mA/cm$^2$ and incorporation of Mn and Ni rise the current density upto a new level with a value of 147.85 mA/cm$^2$. The electrochemical properties of the all prepared

catalysts in comparison with reported electrocatalysts by cyclic voltammograms, current density and scan rate are summarized in the following tabular form.

Table 0.4  Comparison study of prepared samples with literature

| Catalyst Sample | Conc. Methanol (M) | Scan Rate (mV/sec) | Peak potential (Anodic)(V) | Peak Current Density (mA/cm$^2$) | References |
|---|---|---|---|---|---|
| ZnO/CeO(60%,40%)@CNFs | 3 | 50 | 0.4 | 5.3 | [21] |
| Co-Mof | 3 | 50 | 0.10 | 10.4 | [22] |
| ZnO/CeO(40%,60%)@CNFs | 3 | 50 | 0.4 | 16.3 | [21] |
| 2wt%/Co-Mof | 3 | 50 | 0.10 | 17.6 | [22] |
| 5wt%/Co-Mof | 3 | 50 | 0.10 | 29.1 | [22] |
| Co/NPC | 3 | 50 | 0.6 | 28.72 | This work |
| MnCo/NPC | 3 | 50 | 0.6 | 63.35 | This work |
| NiMnCo/NPC | 3 | 50 | 0.6 | 147.85 | This work |

Below is a schematic mechanism of the electrochemical processes for methanol oxidation on the catalyst surface in 3 M methanol and 1 M NaOH [16].

$$Ni\,/\,Mn\,/\,Co\text{-}MIM\,+\,CH_3OH\,\rightarrow\,Ni\,/\,Mn\,/\,Co\text{-}MIM(CH_3OH)_{ads}$$

$$Ni/Mn\,/\,Co\text{-}MIM(CH_3OH)_{ads}\,\rightarrow\,Ni\,/\,Mn/Co\text{-}MIM(CH_2OH)_{ads}\,+\,H^+\,+\,\bar{e}$$

$$Ni/Mn\,/\,Co\text{-}MIM(CH_2OH)_{ads}\,\rightarrow\,Ni\,/\,Mn\,/\,Co\text{-}MIM(CHOH)_{ads}\,+\,H^+\,+\,\bar{e}$$

$$Ni\,/\,Mn\,/\,Co\text{-}MIM(CHOH)_{ads}\,\rightarrow\,Ni\,/\,Mn\,/\,Co\text{-}MIM(COH)_{ads}\,+\,H^+\,+\,\bar{e}$$

$$Ni\,/\,Mn\,/\,Co\text{-}MIM(COH)_{ads}\,\rightarrow\,Ni\,/\,Mn\,/\,Co\text{-}MIM(CO)_{ads}\,+\,H^+\,+\,\bar{e}$$

$$Ni\,/\,Mn\,/\,Co\text{-}MIM\,+\,H_2O\,\rightarrow\,Ni\,/\,Mn\,/\,Co\text{-}MIM(H_2O)_{ads}$$

$$Ni\,/\,Mn\,/\,Co\text{-}MIM(H_2O)_{ads}\,\rightarrow\,Ni\,/\,Mn\,/\,Co\text{-}MIM(OH)_{ads}\,+\,H^+\,+\,\bar{e}$$

$$Ni\,/\,Mn\,/\,Co\text{-}MIM(COH)_{ads}\,+\,Ni\,/\,Mn\,/\,Co\text{-}MIM(H_2O)_{ads}$$

$$\rightarrow\,Ni\,/\,Mn\,/\,Co\text{-}MIM\,+\,CO_2\,+\,3H^+\,+\,3\bar{e}$$

$$Ni\,/\,Mn\,/\,Co\text{-}MIM(H_2O)_{ads}\,+\,Ni\,/\,Mn\,/\,Co\text{-}MIM(CO)_{ads}$$

$$\rightarrow\,Ni\,/\,Mn\,/\,Co\text{-}MIM\,+\,CO_2\,+\,2H^+\,+\,2\bar{e}$$

## Summary

All the results obtained during the research are discussed in this chapter. Characterization results of XRD, SEM, EDS, FTIR, TEM and XPS are supported with facts from previous studies and justified to understand the morphology, structure, composition, thermal stability, functional groups, surface area and porosity of the synthesized materials. Electrochemical results of the synthesized electrodes are discussed at the end. All the results are presented after comparison with the literature and are supported in the light of properties from characterization techniques.

# References

[1]     S. Zhang, Q. Yang, Z. Li, W. Wang, C. Wang, and Z. J. A. Wang, "Zeolitic imidazole framework templated synthesis of nanoporous carbon as a novel fiber coating for solid-phase microextraction," vol. 141, no. 3, pp. 1127-1135, 2016.

[2]     H. Jin, D. Yuan, S. Zhu, X. Zhu, and J. J. D. T. Zhu, "Ni–Co layered double hydroxide on carbon nanorods and graphene nanoribbons derived from MOFs for supercapacitors," vol. 47, no. 26, pp. 8706-8715, 2018.

[3]     B. R. Raju, E. L. Reddy, J. Karuppiah, P. Reddy, M. Kumar, and C. J. J. o. C. S. Subrahmanyam, "Catalytic non-thermal plasma reactor for the decomposition of a mixture of volatile organic compounds," vol. 125, no. 3, pp. 673-678, 2013.

[4]     X. Wang et al., "Synthesis and capacitance properties of N-doped porous carbon/NixCoyOz/carbon micro–nanotubes composites using coal-based polyaniline as a carbon and nitrogen source," vol. 30, no. 2, pp. 1056-1067, 2019.

[5]     M. A. Raza et al., "CoS2/MnS2 co-doped ZIF-derived nitrogen doped high surface area carbon-based electrode for high-performance supercapacitors," Electrochimica Acta, vol. 407, p. 139914, 2022/03/01/ 2022.

[6]     Y. Cao et al., "Sodium Ion Insertion in Hollow Carbon Nanowires for Battery Applications," Nano Letters, vol. 12, no. 7, pp. 3783-3787, 2012/07/11 2012.

[7]     M. V. Tran and P. M. L. J. J. o. N. Le, "Nanoflake manganese oxide and nickel-manganese oxide synthesized by electrodeposition for electrochemical capacitor," vol. 2015, 2015.

[8]     K. M. Racik, K. Guruprasad, M. Mahendiran, J. Madhavan, T. Maiyalagan, and M. J. J. o. M. S. M. i. E. Raj, "Enhanced electrochemical performance of MnO2/NiO nanocomposite for supercapacitor electrode with excellent cycling stability," vol. 30, no. 5, pp. 5222-5232, 2019.

[9]     F. Zhang, C. Yuan, X. Lu, L. Zhang, Q. Che, and X. Zhang, "Facile growth of mesoporous Co3O4 nanowire arrays on Ni foam for high performance electrochemical capacitors," Journal of Power Sources, vol. 203, pp. 250–256, 04/01 2012.

[10]    C. Lamiel, D. R. Kumar, and J.-J. J. C. E. J. Shim, "Microwave-assisted binder-free synthesis of 3D Ni-Co-Mn oxide nanoflakes@ Ni foam electrode for supercapacitor applications," vol. 316, pp. 1091-1102, 2017.

[11]    Y. Wang et al., "Mn3O4/Co (OH) 2 cactus-type nanoarrays for high-energy-density asymmetric supercapacitors," vol. 55, no. 2, pp. 724-737, 2020.

[12]    H. Miao, K. Ma, H. Zhu, K. Yin, Y. Zhang, and Y. J. R. a. Cui, "Ammonia borane dehydrogenation and selective hydrogenation of functionalized nitroarene over a porous nickel–cobalt bimetallic catalyst," vol. 9, no. 26, pp. 14580-14585, 2019.

[13]    Y. Lei et al., "Nitrogen-Doped Porous Carbon Nanosheets Strongly Coupled with Mo2C Nanoparticles for Efficient Electrocatalytic Hydrogen Evolution," vol. 14, no. 1, pp. 1-8, 2019.

[14]    C. Wang, K. Zhang, H. Xu, Y. Du, M. C. J. J. o. c. Goh, and i. science, "Anchoring gold nanoparticles on poly (3, 4-ethylenedioxythiophene)(PEDOT) nanonet as three-dimensional electrocatalysts toward ethanol and 2-propanol oxidation," vol. 541, pp. 258-268, 2019.

[15]    X. Zhang, Z. H. Jiang, Z. P. Yao, Y. Song, and Z. D. J. C. s. Wu, "Effects of scan rate on the potentiodynamic polarization curve obtained to determine the Tafel slopes and corrosion current density," vol. 51, no. 3, pp. 581-587, 2009.

[16]    T. Noor et al., "Nanocomposites of NiO/CuO based MOF with rGO: An efficient and robust electrocatalyst for methanol oxidation reaction in DMFC," vol. 10, no. 8, p. 1601, 2020.

[17]    C. Cordeiro, M. De Vries, T. Cremers, and B. Westerink, "The role of surface availability in membrane-induced selectivity for amperometric enzyme-based biosensors," Sensors and Actuators B: Chemical, vol. 223, pp. 679-688, 2016.

[18]    G. Behmenyar and A. N. J. J. o. P. S. Akın, "Investigation of carbon supported Pd–Cu nanoparticles as anode catalysts for direct borohydride fuel cell," vol. 249, pp. 239-246, 2014.

[19]    W. Huang et al., "Highly active and durable methanol oxidation electrocatalyst based on the synergy of platinum–nickel hydroxide–graphene," vol. 6, no. 1, pp. 1-8, 2015.

[20]    K. Kakaei, M. D. Esrafili, and A. Ehsani, "Graphene and Anticorrosive Properties," in Interface Science and Technology, vol. 27: Elsevier, 2019, pp. 303-337.

[21]   Z. K. Ghouri et al., "Nano-engineered ZnO/CeO2 dots@CNFs for fuel cell application," Arabian Journal of Chemistry, vol. 9, no. 2, pp. 219-228, 2016/03/01/ 2016.

[22]   R. Mehek, N. Iqbal, T. Noor, H. Nasir, Y. Mehmood, and S. Ahmed, "Novel Co-MOF/Graphene Oxide Electrocatalyst for Methanol Oxidation," Electrochimica Acta, vol. 255, pp. 195-204, 2017/11/20/ 2017.

# Chapter 6:

# Conclusions and Recommendations

## 6.1 Conclusions

A simple solution mixing procedure was used to synthesize monometallic Co/NPC, bimetallic MnCo/NPC, and ternary NiMnCo/NPC composites. with organic linker 2-methyl imidazole Surface morphology of prepared samples and presence of specific elements and functional groups were confirmed by SEM, EDS, XPS, TEM, and FTIR. Furthermore, incorporation of metals were also confirmed by XRD.

Electrochemical activity of prepared catalysts was also tested for methanol oxidation reaction (MOR) by using CV, EIS and CA by using three electrode system i.e. GCE as working electrode, Pt wire as counter electrode and Ag/AgCl as reference electrode. The electro-catalytic performance of the catalysts against the MOR process in basic media was examined. For production of hydrogen via methanol oxidation, this research showed that the synthesized catalyst has a significant potential, because of the addition of non-noble catalytic material, making it a cost-effective with the increased activity. The NiMnCo/NPC composite outperformed MnCo/NPC and Co/NPC in terms of impedance, with the greatest peak current density value of 147.85 mA/cm$^2$ at a scan rate of 50mV vs Ag. Because of these exceptional capabilities, this ternary NiMnCo/NPC as a catalytic material is a possible alternative to existing expensive catalysts for hydrogen synthesis from methanol.

## 6.2 Future Recommendations

➢ Effect of other non-noble metals promotion on NiMnCo/NPC can be tested for methanol oxidation reaction.

➢ The NiMnCo/NPC composites can be studied for catalysis of Oxygen evolution reaction (OER).

➢ Effect of temperature on catalytic process of methanol oxidation reaction can also be investigated.

➢ NiMnCo/NPC can also test for $CO_2$ capturing being produce in methanol oxidation reaction.

# Appendix: Publications

## ZIF-67 derived Ternary NiMnCo based Nanoporous Carbon Material for Methanol Oxidation Reaction

Aqsa Saqib Lodhi [a], Naseem Iqbal [a*], Tayyaba Noor [b], Neelam Zaman [a], Junko Gao [c]

## Abstract

In this study, the electrocatalytic activity of mono-metallic Co/NPC, bi-metallic MnCo/NPC, and ternary NiMnCo/NPC in alkaline media for the methanol oxidation process was examined (MOR). These materials were produced using a simple solution mixing method and characterized using FTIR, EDX, SEM, XPS, TGA and XRD. In a three-electrode arrangement, on glassy carbon electrodes, the investigation of methanol oxidation for electrochemical activity of catalysts was carried in 1 M NaOH and 3 M $CH_3OH$. Electrochemical studies included cyclic voltammetry (CV), chronoamperometry (CA), and electron impedance spectroscopy (EIS). The ternary NiMnCo/NPC composite, which has a peak current density of 147.85 mA/$cm^2$ at 0.8 potential and a scan rate of 50 mV/s among all the composites developed, is a promising catalyst for methanol electrocatalysis.